Vincenzo Balzani (Ed.)

Electron Transfer in Chemistry

3 Biological Systems
Artificial Supramolecular Systems

WILEY-VCH

Weinheim · New York · Chichester
Brisbane · Singapore · Toronto

ISBN 3-527-29912-2

© WILEY-VCH Verlag GmbH, D-69469 Weinheim (Federal Republic of Germany). 2001

4 Redox Enzymes: Correlation of Three-Dimensional Structure and Mechanism for Heme-Containing Oxygenases and Peroxidases

Alycen E. Pond, Amy P. Ledbetter, Masanori Sono, David B. Goodin, and John H. Dawson

4 Redox Enzymes: Correlation of Three-Dimensional Structure and Mechanism for Heme-Containing Oxygenases and Peroxidases

Alycen E. Pond, Amy P. Ledbetter, Masanori Sono, David B. Goodin, and John H. Dawson

4.1 Introduction

Heme proteins are arguably the most versatile class of proteins in biology. This group of metalloproteins contains a common heme prosthetic group, yet performs a wide variety of chemical reactions including electron transfer (cytochromes) [1, 2], oxygen activation and insertion (cytochrome P450s) [3–6], oxygen transport (hemoglobin and myoglobin) [3, 7, 8], substrate oxidation (peroxidases and catalases) [9–11], and nitric oxide biosynthesis (nitric oxide synthase) [12, 13]. The heme prosthetic group consists of a highly symmetrical and conjugated protoporphyrin IX macrocycle coordinated to an iron atom [2]. As shown in Figure 1, this group, also termed heme *b*, has two propionate groups, two vinyl groups, and four methyl groups as substituents on the porphyrin ring system. A unique property of the heme prosthetic group is the significant electron and spin delocalization possible among the porphyrin macrocycle, the centrally ligated iron, and the two axial ligands [14–18]. The ability of the porphyrin macrocycle to efficiently redistribute the net atomic charges and unpaired spin density plays a key role in the formation and stabilization of the various heme species required for function [14–18]. Modifications in either the level of conjugation or the substituents on the ring structure influence the electronic properties of the system, and thus result in distinct reactivity and spectroscopic properties [19].

The utilization of heme *b* in the coupling of substrate oxidation to dioxygen or peroxide reduction is seen for three types of heme-containing proteins: oxygenases (Reaction 1A/1B), oxidases (Reaction 2), and peroxidases (Reaction 3). There are two classes of oxygenases where either one oxygen atom from molecular oxygen (or hydrogen peroxide, Reaction 1B) is incorporated into the substrate and the second atom is reduced to water (monooxygenases) or both oxygen atoms are incorporated to give a doubly oxygenated product (dioxygenases). Oxidases and peroxidases do not produce an oxygenated product, rather substrates are oxidized as molecular

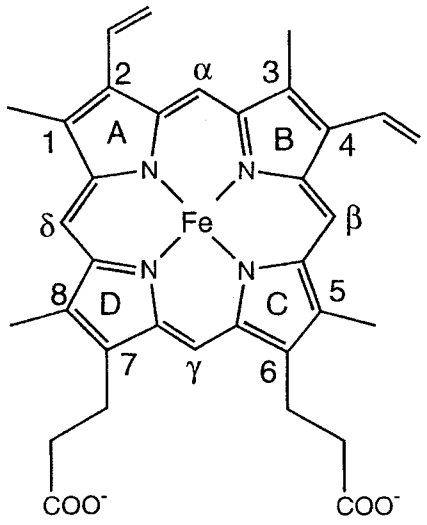

Figure 1. Structure of protoheme IX (iron protoporphyrin IX, heme *b*).

Monooxygenase	$R-H + O_2 + 2H^+ - 2e^- \rightarrow R-OH + H_2O$	(1A)
Peroxygenase	$R-H + H_2O_2 \rightarrow R-OH + H_2O$	(1B)
Oxidase	$2RH_2 + O_2 \rightarrow 2R + 2H_2O$	(2)
Peroxidase	$RH_2 + H_2O_2 \rightarrow R + 2H_2O$	(3)

oxygen or hydrogen peroxide are reduced to water, respectively. While all three classes of enzymes possess the same heme core, their catalytic function varies greatly. The basis for this variance stems from the three factors that control the properties of metals in biological systems: (i) the coordination state of the metal complex; (ii) the nature of the axial ligands in the fifth and sixth coordination sites; and (iii) the protein environment enclosing the metal complex including the polarity of the surroundings and the accessibility of substrates and solvent to the metal [3]. Monooxygenases have various structural features that are not shared by the peroxidases, and vice versa [3]. An understanding of how these differences correlate to enzyme function is essential in defining the relationships between oxygenases and oxidases. In this review we provide updated accounts of the mechanisms of heme-containing monooxygenases and peroxidases, with particular emphasis on the relation of their respective mechanisms to their high-resolution X-ray crystal structures.

4.2 Cytochrome P450

4.2.1 Introduction

The monooxygenase family has the catalytic ability to incorporate an oxygen atom from molecular oxygen to yield a singly oxygenated product while reducing the second oxygen to water. In the years before 1955, the sole role of oxygen in biological systems was believed to be as an electron acceptor in dioxygen-utilizing oxidases or dehydrogenases. In that year, Mason et al. [20] and Hayaishi et al. [21] independently demonstrated through $^{18}O_2$ labeling experiments that one or both oxygen atoms from molecular oxygen can be incorporated into organic molecules following enzymatic oxidation. The enzymes that incorporate oxygen atoms from dioxygen were termed "oxygenases" by Hayaishi [22]. Shortly after the discovery of oxygenases and their enzymatic activity, Garfinkel [23] and Klingenberg [24] independently described the presence of a carbon monoxide (CO)-binding pigment in liver microsomes, which exhibited unusual absorbance maxima near 450 nm in the ferrous-CO minus ferrous difference spectrum. Omura and Sato [25] later identified this pigment ("P") as a heme protein containing a protoporphyrin IX (Figure 1) prosthetic group and assigned it the name "cytochrome P450".

Enzymes of the P450 superfamily are by far the best characterized of all heme-containing monooxygenases, and are extensively distributed throughout the plant, animal, and microorganism kingdoms. To date, more than 500 isozymes have been cloned and sequenced with enzymatic activities covering a vast variety of reactivities including hydroxylation of inactivated alkanes, conversion of alkenes to epoxides, arenes to phenols, and sulfides to sulfoxides to sulfones (Figure 2). The hydroxylation of various harmful organic molecules by P450 enzymes greatly increases the solubility of the organic substrate, thereby facilitating their excretion from biological systems. In contrast to their beneficial roles, P450 enzymes can also transform certain otherwise nonreactive molecules such as benzo(a)pyrene into highly reactive carcinogens [3], making P450 enzymes attractive targets for cancer-related drug design and development.

With the exception of microbial P450 enzymes, the majority of P450 proteins are membrane-bound, being associated with either the inner mitochondrial or endoplasmic reticulum (microsomal) membrane. Initial efforts to release the membrane-bound P450s from the membrane by detergent solubilization led to a loss of monooxygenase reactivity, as well as a shift the characteristic 450 nm absorbance peak to 420 nm in the difference spectrum [25]. Subsequently, successful solubilization and purification of the active form of the P450 proteins and associated electron transport proteins were achieved for the mitochondrial and microsomal P450s by Estabrook and Coon and their respective coworkers [26, 27]. Gunsalas and coworkers [28] discovered a soluble camphor-inducible bacterial monooxygenase P450 (P450CAM) system in *Pseudomonas pituda*. The solubility of P450CAM allows large quantities to be purified for detailed mechanistic and spectroscopic studies, as well as successful crystallographic analysis. The crystal structure determined by Poulos and coworkers [29–33] provides researchers with a model to study

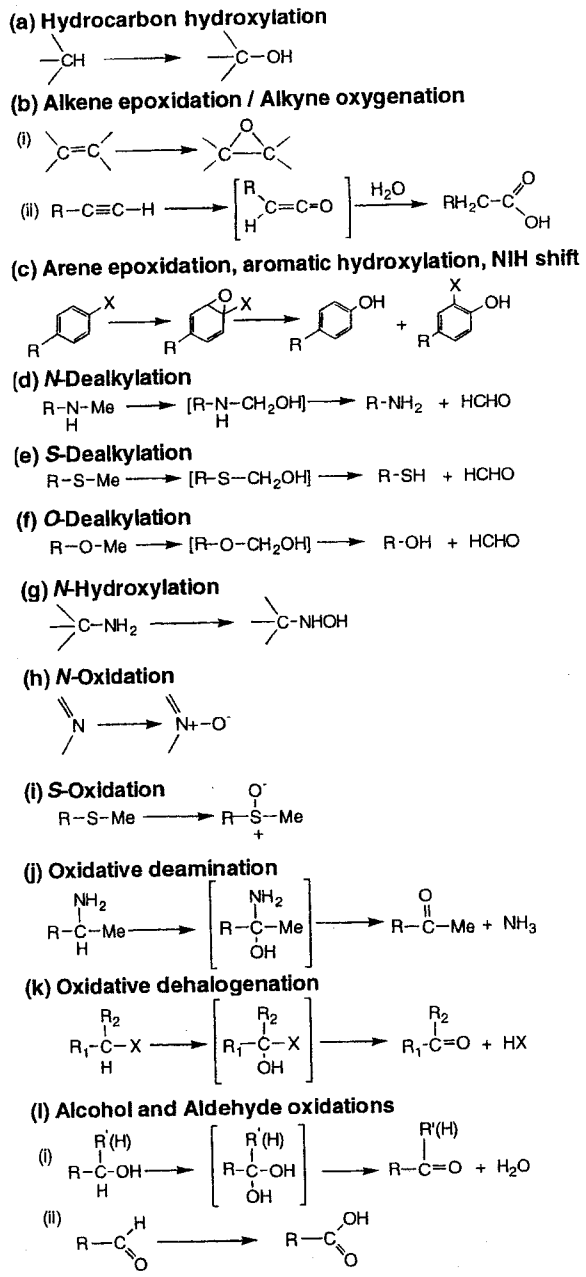

Figure 2. Schematic summary of some of the diverse P450-catalyzed reactions. (Adapted from Ref. [6].)

the relationship between the P450s and their substrates, making P450CAM the preferred vehicle for studying the relationship between structure and function of the P450 family.

4.2.2 Reaction Cycle of P450

Electron transport systems

In catalyzing its monooxygenase reaction, P450 can utilize either NADH or NADPH as an electron source. The electron transport system varies among the P450 proteins, and thus allows for an organization of the superfamily into smaller classes. Most bacterial and mitochondrial P450 systems are termed Class I P450s, utilizing flavin and iron–sulfur prosthetic groups for electron transfer from NAD(P)H [34]. Figure 3A illustrates such a system where reducing equivalents flow from NAD(P)H to a FAD-containing protein to an iron–sulfur protein to the P450. Microsomal systems are termed Class II P450s and employ a single flavoprotein, NADPH-cytochrome P450 reductase, containing both FAD and FMN components to shuttle electrons from NADH to the P450 (Figure 3B) [34]. P450BM-3 is an unusual bacterial P450 from *Bacillus megaterium* that is a natural fusion protein consisting of a P450 domain and a NADPH-cytochrome P450 reductase domain that enables the protein to be self-sufficient (Figure 3C) [34, 35]. Finally, P450nor from *Fusarium oxysporum* is a Class IV P450 that appears to accept electrons directly from reduced pyridine nucleosides without intervening electron carriers (Figure 3D) [36].

The reaction cycle and intermediates

The common feature of P450 enzymes is their utilization of a cysteinate-ligated heme active site to catalyze their respective monooxygenase chemistry. The monooxygenation reaction catalyzed by P450CAM in the hydroxylation of (1*R*)-camphor is shown in Reaction 4. The reaction cycle determined for P450CAM (Figure 4) is likely shared by most members of the P450 family [37], and involves four well-characterized and isolatable complexes, **1**–**4**, [4, 37]. The substrate-free resting state, **1**, is six-coordinate low-spin with a proximal cysteine residue from the protein and a distal water molecule from the solvent serving as the axial ligands (Figure 5B). Addition of camphor displaces the solvent molecule, yielding a five-coordinate high-spin complex, **2**, with a vacant coordination site on the distal side of the heme that will ultimately be available for dioxygen binding. The shift of the iron spin

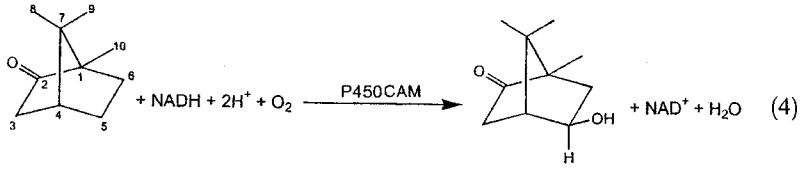

(4)

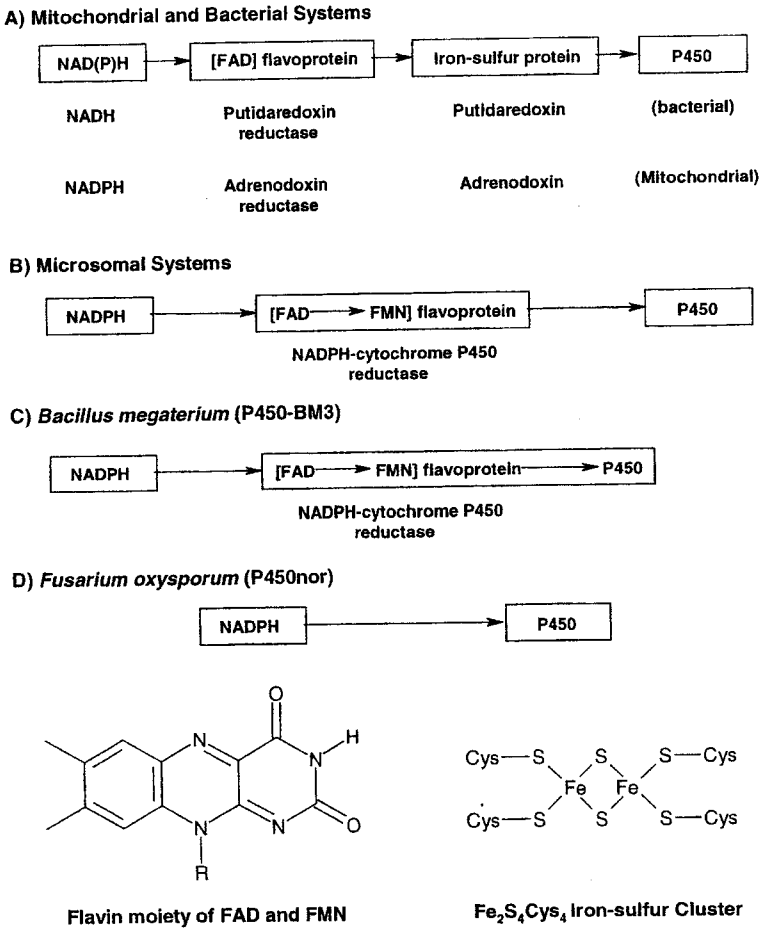

Figure 3. Electron donors and transport pathways for A) mitochondrial and bacterial; B) microsomal; C) *Bacillus megaterium*; and D) *Fusarium oxysporum* P450 systems. The structures of the flavin moiety of FAD and FMN (bottom left) and the $Fe_2S_2Cys_4$ cluster (bottom right).

state from low- to high-spin upon substrate binding results in a significant increase in the redox potential ($E^{o\prime}$) of the heme iron (−330 to −173 mV versus NHE). As seen in Reaction 1A, the activation of molecular oxygen for monooxygenase chemistry requires the input of two electrons. For P450CAM, these electrons are provided by NADH via two electron transport proteins (Figure 3A): putidaredoxin reductase (a FAD-containing protein) and putidaredoxin (an iron–sulfur protein). Substrate binding facilitates electron donation from the reduced putidaredoxin

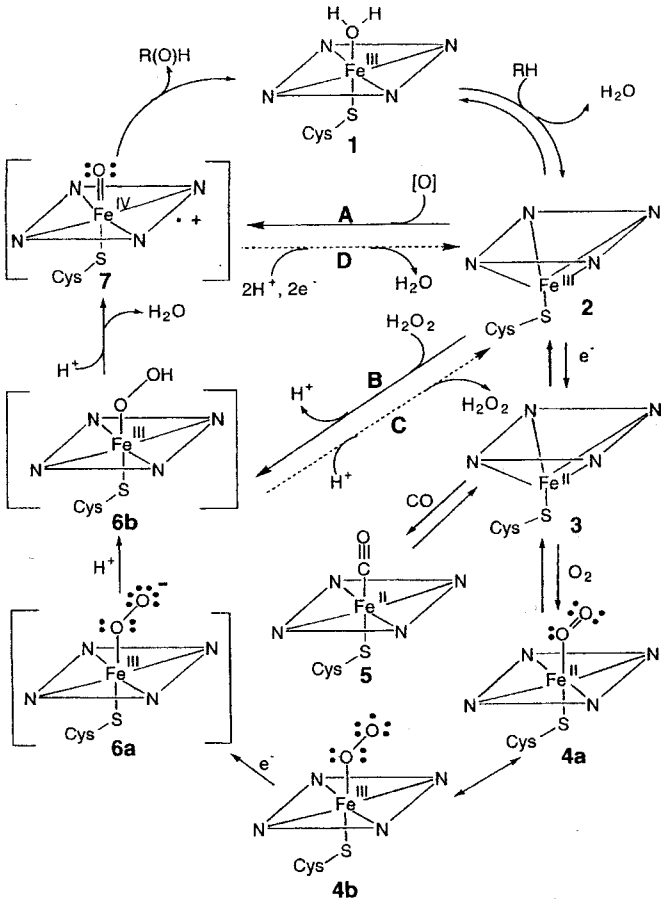

Figure 4. Catalytic cycle of cytochrome P450 including the postulated structures of the putative intermediates. RH represents the substrate and R(O)H represents the product. The porphyrin macrocycle is abbreviated as a parallelogram with nitrogens at the corners. See text for details. (Adapted from Ref. [6].)

($E^{o\prime} = -196$ mV) to the ferric P450CAM heme iron to produce the ferrous state of the protein, **3**. Dioxygen binds to the ferrous heme iron to form the ferrous oxy complex, **4a/4b**, whose valence structure can be presented either as the ferrous-O_2, **4a**, or as the ferric superoxide, **4b**, complex. Addition of carbon monoxide to **3** yields a ferrous carbon monoxide adduct, **5**, with its characteristic absorbance peak at 450 nm [37].

Addition of a second electron from NADH, **4a/4b**, the rate-limiting step of the

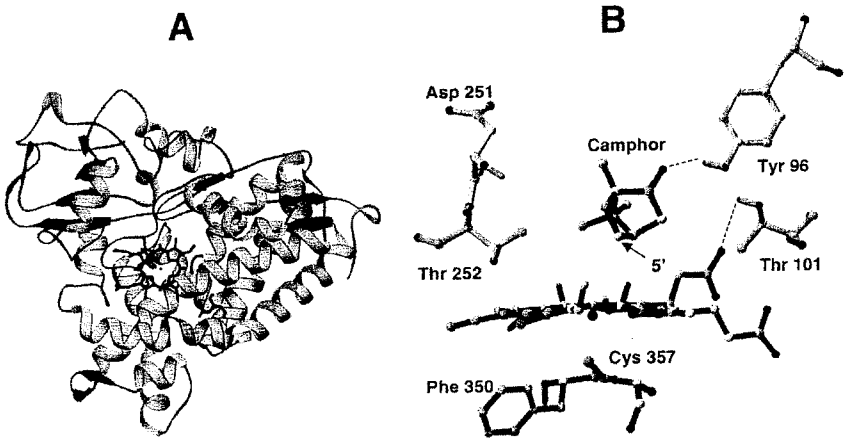

Figure 5. (A) Schematic representation of the crystal structure of P450CAM generated from the X-ray coordinates [58]. Helical regions, β-sheet regions, and the heme group are shown. (B) Key catalytic residues and the location of camphor in the heme active site [58]. The heme is ligated to a cysteine residue with the sixth position vacant. Dashed lines represent hydrogen bonding interactions between the C2 carbonyl of camphor and Tyr96, and the heme propionate and Thr101. The site of hydroxylation on the camphor molecule is denoted with an arrow.

catalytic cycle [38, 39], is proposed to give a ferric peroxide complex, **6a**, which can then be protonated to yield a ferric hydroperoxide species, **6b**. Addition of a second proton to this outer oxygen leads to heterolytic cleavage of the O–O bond, releasing water and generating the proposed oxo-ferryl ($O=Fe^{IV}$) porphyrin radical intermediate, **7**. Intermediate **7** is equivalent to the high-valent iron-oxo species of the peroxidases called Compound I. Compound I is the most likely candidate for the "reactive oxygen" form of P450 that hydroxylates inactivated hydrocarbon substrates. Abstraction of a hydrogen atom from the substrate by **7** forms a substrate-based carbon radical and an iron-bound hydroxyl radical. Radical rebound then yields the hydroxylated product and regenerates **1** [3, 4, 6, 40].

The short circuit or peroxide shunt

The cycle can also be turned over by two shunt pathways (pathway **A** and **B** in Figure 4). First, oxygen atom donors ([O]) such as iodosobenzene and peracids can replace the two electrons and dioxygen required for the normal catalytic cycle and react directly with **2** to generate oxygenated products likely through intermediate **7** (Pathway **A**) [4, 27, 41]. Similarly, some P450 proteins are able to replace molecular oxygen and NADH with hydrogen peroxide in a manner similar to the peroxidases. Pathway **B** illustrates the utilization of hydrogen peroxide to form **7** from substrate-bound ferric P450CAM (**2**) via the ferric hydroperoxide species, **6b** (4). Conversely,

pathways **C** and **D** illustrate the uncoupling of NADH oxidation and oxygen transfer. Protonation of the iron bound oxygen in **6b** releases hydrogen peroxide generating the five-coordinate ferric state, **2**, with no oxygen transfer to substrate (pathway **C**), a two-electron uncoupling reaction. Also, two-electron reduction and diprotonation of the oxo group in **7** gives a second molecule of water, regenerates complex **2**, and no oxygenated product yielding a four-electron uncoupling reaction (pathway **D**) [42–44].

Poulos has discussed the most likely causes of these latter two uncoupling reactions based on examination of the crystal structures of complexes of P450CAM with various camphor analogues and of site-directed mutants of P450CAM with modified substrate-binding sites [45]. The presence of excess solvent molecules near the heme, as well as an increase in substrate mobility, have been suggested as possible explanations for the uncoupling of electron transfer to oxygen transfer. Despite being the ultimate source of the protons needed for catalytic turnover, the presence of excess solvent within the active site could promote various uncoupling reactions. In related work, Sligar and coworkers have demonstrated that steric factors on the distal side of the heme strongly influence the coupling of oxygen and electron transfer in P450CAM and the partitioning between two- and four-electron uncoupling [42].

4.2.3 Molecular Structure of P450

In 1985, P450CAM was the first P450 protein to be successfully crystallized and have its structure determined [29]. The protein has an asymmetrical triangular shape consisting of 12 α helices and five anti-parallel β sheets (Figure 5A). The heme prosthetic group is deeply embedded into the hydrophobic interior of the protein, sandwiched between two long α helices, with no significant exposure to the surface of the protein. Previous spectroscopic investigations of P450CAM established that a cysteine residue serves as the endogenous ligand donated by the protein [4]. This finding was substantiated by the crystal structure identifying Cys357 as the proximal ligand to the heme (Figure 5B). Several years later, the structure of the P450 domain of P450BM-3 was determined [46], giving researchers models for a class I (P450CAM) and a class II (P450BM-3) P450. A side-by-side comparison of these two proteins can be seen in Figure 6. Subsequently, the successful crystallization and crystallographic analysis of two other class I P450s, P450TERP [47] and P450eryF [48, 49], a class IV P450, P450nor [50, 51], and P450csa [52] have been achieved. Additional structures of P450CAM and P450BM-3 in various coordination states and oxidation states [53–55] and several mutant forms of P450CAM [56–58] are also available.

Comparison of the amino acid sequences of members of the P450 family has revealed two areas of sequence similarity [59]. One region contains the proximal cysteine ligand along with the residues comprising its binding pocket. The second area of conservation corresponds to Thr252 of P450CAM located on helix I, which interacts directly with the bound dioxygen molecule of the P450–O_2 complex (Figure 5B). Both these areas are vital for efficient catalytic turnover, and will be discussed in later sections. With the availability of the structural data of the above

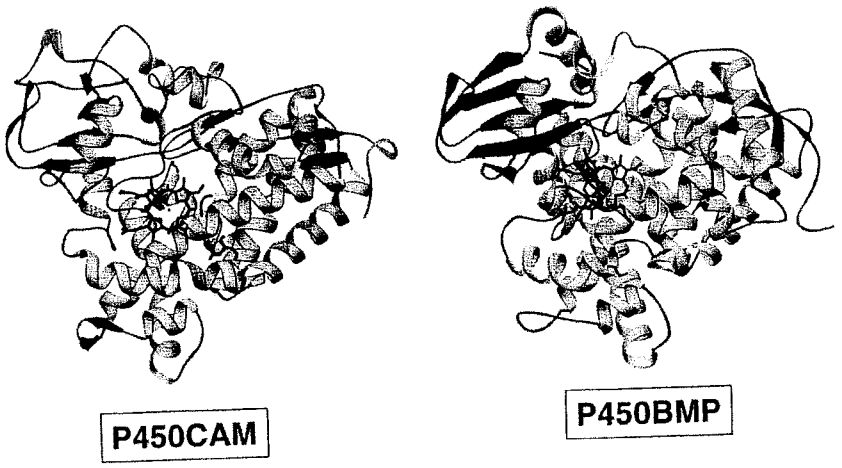

Figure 6. A side-by-side comparison of the secondary structures of P450CAM (left) and P450BM-3 (right) generated from their respective X-ray coordinates [58, 210]. Helical regions, β-sheet regions, and the heme group are shown.

P450s, it appears that the overall structural protein fold and the spatial organization of the heme-binding site are highly conserved, despite a less than 20% sequence identity among the proteins. Closer examination of these structures shows that there is ample diversity in the primary, secondary, and tertiary structures of the proteins to accommodate their wide variety of substrates, redox partners, and cellular locations. Detailed structural comparisons of these P450 proteins by Poulos et al. [33] and Peterson and colleagues [34, 59] can be found in the P450 literature.

In this new millennium, significant advancements have already been made in the crystallographic study of P450 proteins. First, McRee and coworkers produced the first X-ray crystal structure of a microsomal P450, P450 2C5 [60]. Comparison of this structure with those of microbial P450s indicates that the overall fold of the two types of P450 proteins is similar, as is the structural core surrounding the heme-binding site. However, significant structural differences exist between the substrate binding sites, and the modes of interaction with both electron donors and the membrane. Close analysis of the P450 2C5 structure provides a basis for the study of the interaction of a microsomal P450 with the endoplasmic reticulum, its substrate, and its redox partner. McRee and coworkers suggest a monofacial attachment of P450 2C5 to the membrane via a broad, hydrophobic surface that is adjacent to the anchor provided by a transmembrane helix at the N terminus [60]. The orientation of P450 2C5 relative to the membrane positions the electrostatic dipole of the P450 in such a manner to maximize the attraction between the protein and its reductase [60]. The entrance to the substrate access channel is located in the membrane attachment surface, suggesting that lipophilic substrates and products can enter or exit the P450 directly from the bilayer. An alternative substrate access

channel is also present, which would allow more water-soluble metabolites to exit directly into the cytoplasm [60]. As there is high sequence similarity between P450 2C5 and 91 other members of family 2 P450 enzymes [60], this structure and its analysis will provide researchers with a template by which to model the interactions of other microsomal P450s.

In a second crystallographic stride forward, Schlichting et al. have obtained structures for previously nonisolatable intermediates in the hydroxylation reaction of camphor by P450CAM utilizing trapping techniques and cryocrystallography [61]. The structure of the oxyferrous complex (**6a**) has been determined to a 0.91 Å resolution, showing a dioxygen molecule which binds end-on to the heme iron with the outer oxygen atom pointing towards Thr252. The bond distance between the heme iron and the inner oxygen is 1.8 Å with a Fe–O–O tilt angle of 132° [61], in agreement with previous extended X-ray absorption fine structure (EXAFS) [62] and resonance Raman [63] studies. In addition to altering the electron density surrounding the heme group, the binding of dioxygen also affects the distal binding pocket in two crucial ways. First, a new ordered solvent molecule (WAT 901) is now present near both the outer oxygen atom and the hydroxyl group of Thr252. Secondly, the backbone atoms of the highly conserved Asp251 and Thr252 have undergone a conformational change in which the carbonyl of Asp251 has flipped 90° towards Asn255, and the amide nitrogen of Thr252 has rotated towards the heme pocket [61]. These alternations result in new hydrogen-bonding interactions among the distal protein residues that appear to stabilize the new solvent molecule, WAT 901.

The addition of a second electron through irradiation of crystals of the oxyferrous complex with long-wavelength X-rays alters the electron density at and around the P450 active site [61]. Difference maps suggest that cleavage of the dioxygen bond has occurred, leaving a single oxygen atom bound to the heme iron. The electron density above the heme is too small to accommodate two oxygen atoms, and is best fit with a single oxygen atom bound to the heme at a distance of 1.65 Å [61]. This distance is much shorter than the 1.8 Å distance of an iron–oxygen single bond, and is in close agreement with computational (1.66 Å) [64] and EXAFS measurements for an oxo ferryl complex in a peroxidase [65]. This potential glimpse of compound I gives credence to the proposed catalytic mechanism of P450CAM and may translate to other P450 systems.

4.2.4 Mechanism of Oxygen Activation

A distinguishing characteristic of monooxygenases and peroxidases from the globins is the ability of the former two proteins to heterolytically cleave the O–O bond (Reaction 5A), while the latter utilize homolytic cleavage (Reaction 5B). This subtle difference in mechanism allows monooxygenases and peroxidases to perform their wide variety of catalytic activities, while globins serve as oxygen carriers. As can be seen in Reactions 5A and 5B, the high-valent Compound I species is formed only when both electrons in the O–O bond go with the leaving group, i.e., heterolytic cleavage. When the bond is cleaved homolytically, as seen for the globins, the

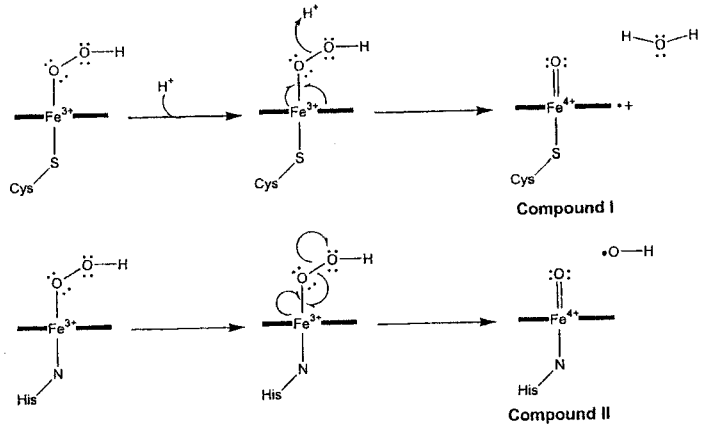

(5A)

(5B)

electrons in the bond are split between the two oxygen atoms, forming Compound II, a less reactive oxo intermediate. The ability of monooxygenases and peroxidases to cleave the O–O bond heterolytically is a direct result of their respective active site protein environments, particularly the proximal ligand and catalytically active protein residues on the distal side of the heme.

The "push–pull" mechanism of the peroxidases

Heme-containing peroxidases carry out heterolytic O–O bond cleavage starting from the ferric state and binding hydrogen peroxide to form the high-valent iron-oxo intermediate, Compound I. The crystal structure of cytochrome *c* peroxidase, a prototypical heme-containing peroxidase, led Poulos to propose a "push–pull" mechanism for the formation of Compound I [66]. In this system, it is proposed that heterolytic cleavage is achieved by a combination of electron density "push" from the anionic proximal histidine, and "pull" by the distal histidine and arginine couple (Figure 7) [66, 67]. The "push" is provided by the proximal histidine ligand whose electron donor capabilities are enhanced due to a strong hydrogen-bonding interaction (partial deprotonation) with a neighboring carboxylate group, thereby increasing its imidazolate character relative to the corresponding histidine ligand of hemoglobin or myoglobin. This anionic character may also serve to stabilize the higher oxidation states of the heme iron during catalysis. Simultaneously, the distal histidine accepts a proton from the inner oxygen of the bound hydrogen peroxide and transfers it to the outer oxygen to generate a good leaving group. The distal histidine works in concert with a strategically positioned cationic arginine residue that serves to stabilize the developing anionic charge on the outer oxygen during bond cleavage. The combination of the distal histidine and arginine provide the "pull" effect. Recent site-directed mutation of residues on both the proximal and distal side supports the push–pull effects on the formation of Compound I of CCP

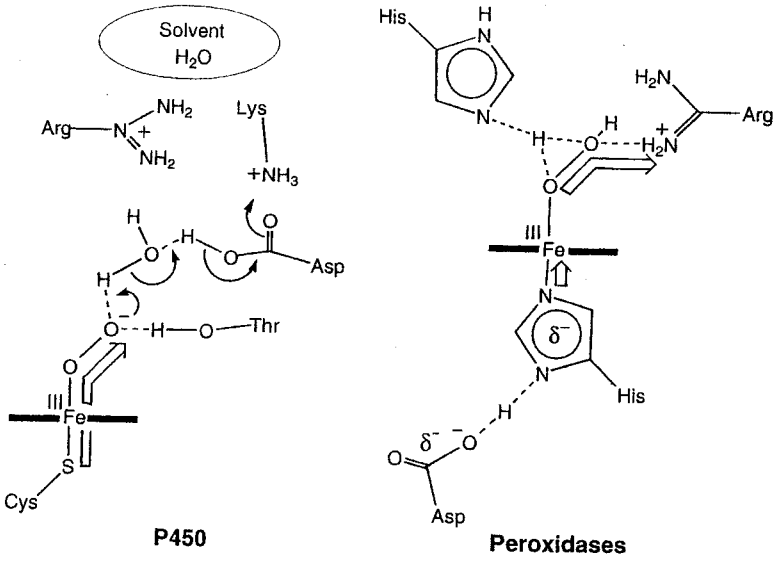

Figure 7. Schematic view of the "push-pull" mechanism for O–O bond cleavage of an iron-bound peroxide in thiolate-ligated (left) and histidine-ligated (right) systems such as P450 and HRP, respectively. (Adapted from Ref. [6].)

[66–71], especially the replacement of the distal histidine with a leucine residue which suppressed the rate of Compound I formation 10^5-fold [67, 69, 70].

The "push" effect of the proximal cysteine ligand for P450

Nearly 25 years ago, Dawson proposed that the P450 proximal thiolate ligand serves as a strong internal electron donor to facilitate O–O bond cleavage to generate Compound I (Figure 7) [72]. Three lines of evidence for the "push" of the cysteinate ligand have been reported. First, bound distal thiolates show enhanced basicity *trans* to the endogenous cysteinate of P450CAM relative to parallel myoglobin adducts [73]. Second, significant differences have been reported for the affinities of anionic ligands to ferric P450 and myoglobin, with anionic ligands having much lower affinity for ferric P450CAM than ferric myoglobin, presumably due to the anionic character of the proximal thiolate ligand [74]. Finally, Dawson and coworkers have observed shifts in the in the X-ray absorption energies for thiolate-ligated heme iron derivatives relative to those lacking a thiolate ligand to provide a direct measure of the strong electron-releasing nature of the thiolate axial ligand [75]. More recently, studies using a His → Cys myoglobin mutant [76] or a thiolate-ligated porphyrin model system [77] demonstrate that the thiolate-ligated systems favor the heterolytic cleavage of the O–O bond compared to wild-type myoglobin

and neutral histidine-ligated porphyrin models that predominantly cleave the O–O bond homolytically. Once the O–O bond is cleaved heterolytically, the anionic character of the thiolate ligand helps to stabilize the high-valent nature of Compound I.

In 1999, Hager and coworkers provided the first evidence that the strong anionic character of the thiolate ligand may not be the only determining factor in the differentiation between homo- and heterolytic cleavage of the O–O bond. Replacement of the proximal thiolate ligand in the related peroxidase enzyme of chloroperoxidase (CPO), a versatile heme enzyme from *Caldariomyces fumageo*, with a histidine resulted in a recombinant mutant that retains most of its chlorination, peroxidation, epoxidation, and catalase activities [78]. This retention of activity despite the loss of thiolate ligation indicates that the environment of the distal pocket may play as important a role as the proximal ligand in differentiating between homo- and heterolytic cleavage of the O–O bond. CPO has a very polar distal environment that is typical of peroxidases. As evidenced by the high activity levels of the Cys → His mutants, this polar environment likely plays a major role in maintaining the diverse catalytic activities of this enzyme.

The proton shuttle in P450

The "push" of the thiolate ligand cannot, by itself, accomplish heterolytic cleavage of the O–O bond (Figure 7). In addition, there must be a source of protons to enable the outer oxygen atom of the bound peroxide (Figure 4, species **6a**) to leave as water. Theoretical studies by Loew and Harris [64] indicate that the protonation of the outer oxygen leads to significant weakening of the O–O bond. This weakening is manifested in both an increase in O–O bond length from 1.33 to 1.46 Å, and a decrease in the bond order from 0.87 to 0.48 [64]. However, only the addition of the second proton results in the cleavage of the dioxygen bond, resulting in the formation of Compound I [64]. These results provide strong support for consecutive or simultaneous double protonation of the outer oxygen atom of the ferrous dioxygen complex being the ultimate cause of O–O bond breakage.

Extensive study of the P450CAM active site has identified two potential routes for proton transfer (Figure 8). The first involves two highly conserved residues, Thr252 and Asp251 [58, 79–83]. The second possibility is via a water chain and the highly conserved Glu366 [84]. Sligar and coworkers have proposed that Thr252 and Asp251 form a proton relay network that works in conjunction with two other charged amino acids to reach the surface solvent and provide a conduit for protons [58, 80–83]. Replacement of Thr252 with alanine (T252A) results in a drastic drop in hydroxylation activity (~95 %) without a simultaneous decrease in NADPH and O_2 consumption (i.e., increased uncoupling) [82, 85]. Similarly, replacement of the corresponding Thr268 with alanine (T268A) in P450BM-3 results in a decrease in substrate (laurate) hydroxylation (~85 %) and an increase in uncoupling [86]. However, in P450CAM substituting Thr252 with either a serine or an O-Me-Thr residue produces an enzyme that retains high activity [79, 87]. The mechanistic results obtained with these mutants indicate that the role of Thr252 in the hydroxylation mechanism is to provide a hydrogen bond rather than a proton during

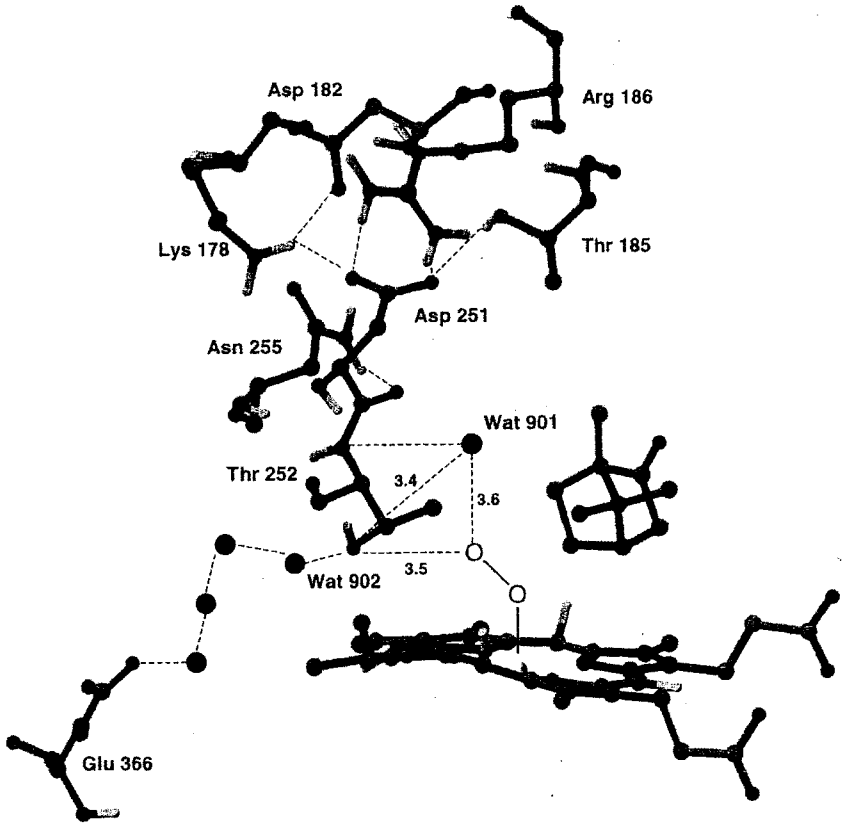

Figure 8. A schematic view of the proposed proton shuttle in the distal pocket of P450CAM. Distal residues and the heme were generated using the X-ray coordinates [58]. Dashed lines represent hydrogen-bonding interactions as determined in Ref. [61]. Water molecules are represented by isolated spheres, with WAT 901 and WAT 902 in positions determined in Ref. [61].

turnover (Figure 8). The recent crystal structure of the oxyferrous complex of P450CAM confirms this assignment, showing Thr252 within hydrogen bonding distance to the bound dioxygen molecule as well as a potentially catalytic solvent molecule, WAT 901 [61].

Replacement of Asp251 with asparagine (D251N) decreases the rate of hydroxylation by two orders of magnitude, with relatively little uncoupling and shifts the rate limiting in the catalytic cycle [58, 80, 88]. Based on isotopic and crystallographic studies of wild-type and D251N P450CAM, Sligar and coworkers proposed a proton shuttle involving two new solvent molecules in the active site, with Asp251 serving as a "caboxylate switch" between solvent-accessible residues and the catalytic water molecules (Figure 8) [79]. However, the availability of recent structural data has altered this proposal somewhat, with Asp251 now serving as a "carbonyl switch" that stabilizes WAT 901 instead [61].

The intrinsic diversity of the family must be kept in mind when trying to apply results for P450CAM to the P450 superfamily. In P450eryF, a P450 that catalyzes the hydroxylation of 6-deoxyerythronolide, there is an alanine (Ala245) in the position corresponding to Thr252 in P450CAM. Mutation of this residue in P450eryF to a threonine (A245T) results in a dysfunctional protein, similar to the opposite mutation in P450CAM (T252A). Therefore, P450eryF must utilize a varied source of protons in its catalytic cycle. Molecular dynamic simulations by Harris and Loew [64, 84] have identified a stable hydrogen-bonding network leading from the outer oxygen of the iron-bound dioxygen to the carboxylic oxygen of Glu360, a highly conserved residue in the P450 family. This residue is located in a solvent-accessible channel, and is likely the ultimate source of protons in P450eryF [64, 84]. The corresponding residue in P450CAM, Glu366, does not appear to serve the same purpose in the catalytic cycle as its mutation to a methionine shows little effect on catalytic activity [89]. Instead, structural data suggest that this residue may "anchor" a solvent chain that extends between Thr252 and Glu366 (Figure 8) [61]. Therefore, neither the role of a specific amino acid nor the consequence of a mutation can be inferred for one P450 enzyme based on the results for another isozyme.

4.3 Nitric Oxide Synthase

4.3.1 Introduction

Nitric oxide (•NO) is a diatomic, reactive radical that has become the focus of intense scientific investigation during the past two decades. Its role as a biological messenger places this small molecule at the heart of a number of complex regulatory mechanisms in diverse biological systems. The ability of •NO to diffuse freely from its point of origin rather than using classical biological trafficking routes (i.e., specific transporters or channels) makes regulation dependent on its actual biosynthesis, and not its movement through the body. Before 1981, •NO biosynthesis was believed to the restricted to bacteria that engaged in nitrification and denitrification reactions [90]. For the first time in 1981, nitrogen oxides were conclusively demonstrated as significant products in mammalian metabolism [90]. Building on this discovery, numerous research groups have focused on the role of •NO in mammalian systems. Stemming from this research, •NO has been implicated as a neurotransmitter in the brain, a vasodilator in smooth muscles, and an immunocytotoxic reagent in macrophages [90]. As the potential functions of •NO become more established, scientific attention has shifted towards its regulation and therefore to the enzyme responsible for its biosynthesis, nitric oxide synthase (NOS). Following initial sequencing and development of a recombinant system in 1991, the amount of knowledge accumulated about NOS is astounding.

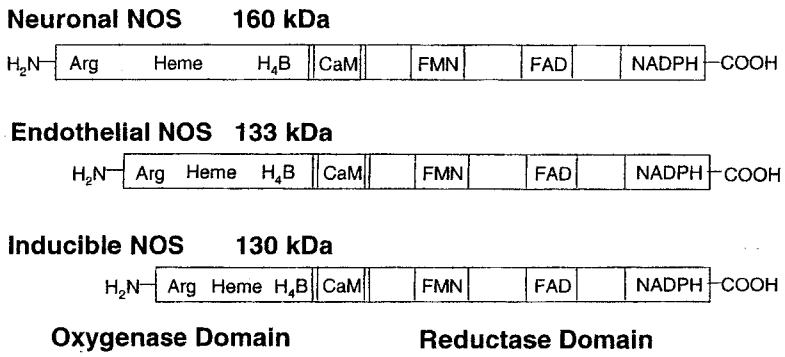

Figure 9. Map of the primary amino acid sequence of nNOS, eNOS, and iNOS. A calcium–calmodulin binding region separates the oxygenase and reductase domains. The reductase domain contains binding sites for two flavin cofactors (FAD and FMN) as well as a binding site for the electron donor, NADPH. The oxygenase domain contains binding sites for the heme, the substrate (L-arginine), and tetrahyrobiopterin (H_4B). (Adapted from Ref. [90].)

4.3.2 The Isoforms

To date, three isoforms of NOS have been identified: neuronal NOS (nNOS, NOS-I, brain), inducible NOS (iNOS, NOS-II, immune system), and endothelial NOS (eNOS, NOS-III, cardiovascular system). These isoforms have been purified from different sources, and many have been cloned and functionally expressed [91]. Each isoform of NOS is comprised of a N-terminal oxygenase domain and a C-terminal reductase domain connected by a 30-amino acid recognition sequence for the binding of the calcium/calmodulin (Ca^{2+}/CaM) complex (Figure 9) [12, 90, 92–95]. The oxygenase domain contains binding sites for the heme, the cofactor tetrahydrobiopterin (H_4B), and the substrate, L-arginine (L-Arg). The reductase domain contains binding sites for NADPH, flavin mononucleotide (FMN), and flavin-adenine dinucleotide (FAD) that shuttle electrons to the heme center to couple product formation. The Ca^{2+}/CaM complex acts as a hinge between the oxygenase and reductase domains, allowing communication between domains [96, 97]. In nNOS and eNOS, the electron flavin-to-heme transfer must be initiated by the binding of the Ca^{2+}/CaM complex, whereas iNOS is active at all times because Ca^{2+}/CaM is always bound. Recently, work with iNOS indicates that the electrons flow between the oxygenase and reductase domains on adjacent subunits (Figure 10) [98]. This "domain swapping" provides a means for NOS to prevent uncoupling of NADPH oxidation and may provide a way for H_4B function or Ca^{2+}/CaM control of heme iron reduction [98].

Dimerization of the oxygenase domains is essential for catalytic activity and for binding of the pterin cofactor [99]. Recent structural data for the dimeric oxygenase domains of NOS [100–102] reveal an extensive dimer interface that creates binding sites for the two pterins, sequesters the heme from the solvent, and helps to structure the substrate binding site (Figure 11). Upon dimerization, all three isoforms pro-

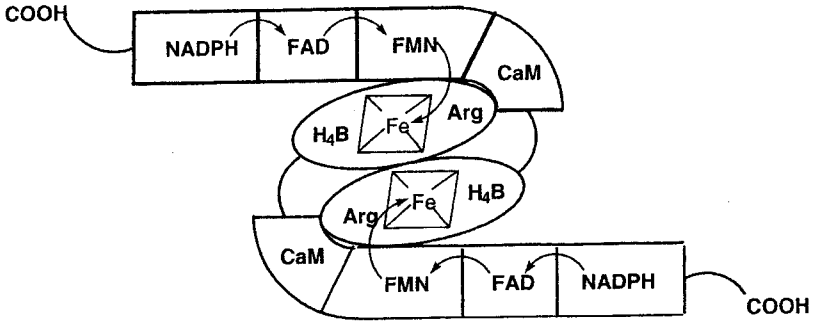

Figure 10. Proposed model for the iNOS dimer indicating domain swapping and electron transfer pathway. (Adapted from Ref. [98].)

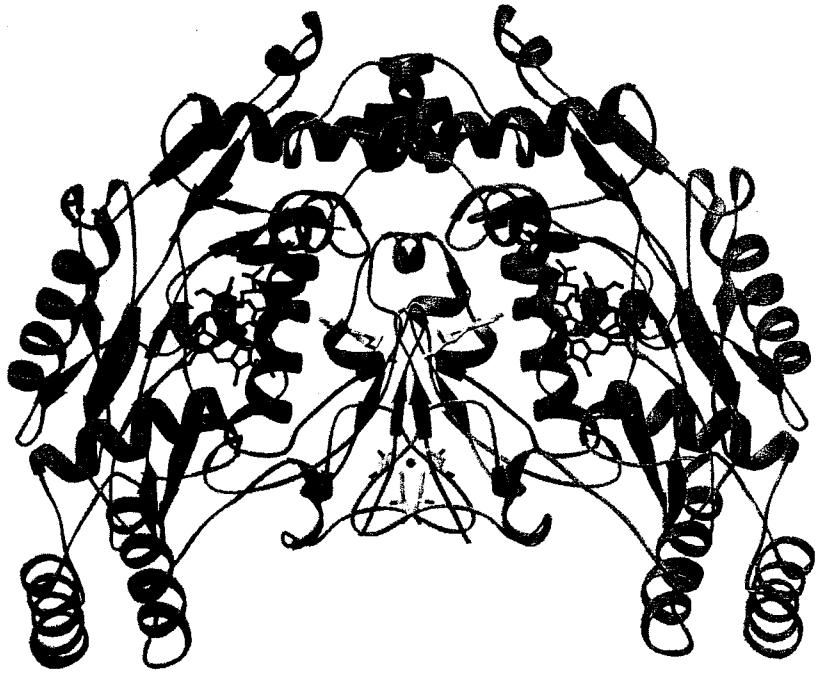

Figure 11. Schematic ribbon drawing of the iNOS oxygenase dimer generated from the X-ray coordinates [107] illustrating the locations of heme, L-arginine, tetrahydrobiopterin, and the zinc ion. The zinc ion is tetrahedrally coordinated to its protein ligands.

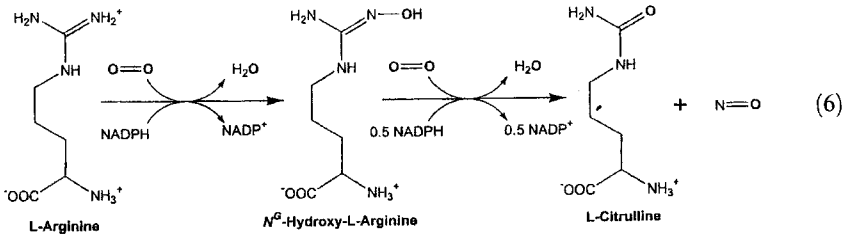

(6)

duce •NO by catalyzing the oxidation of L-arginine to L-citrulline and •NO, via the intermediate, N^{ω}-hydroxy-L-arginine (NHA) (Reaction 6) [12, 92, 95]. The reaction is a variation on the hydroxylation reaction catalyzed by P450 enzymes; thus, it is not surprising that NOS and P450 are very similar biological machines. Both have a thiolate-ligated heme prosthetic group at their respective active sites, and utilize a FMN/FAD reductase system for electron transport from NADPH. With an exception of P450 BM-3, NOS is distinct from P450s in that NOS is a "self-sufficient" monooxygenase in which both the oxygenase and reductase domains are part of a single peptide. Unlike P450 BM-3 that is also self-sufficient by having a fused oxygenase and reductase domains in a single peptide [103], NOS employs a H_4B group, the function of which is poorly understood. However, it is required for efficient catalysis, and essential for •NO production [104].

Neuronal production of •NO is triggered when an activated neuron releases a chemical messenger (glutamate) from the presynaptic neuron to bind to receptor sites (*N*-methyl-D-aspartate) on the postsynaptic neuron. The transmission of this nerve impulse opens a channel in the receptor allowing the influx of calcium ions. These ions can then bind to calmodulin already present in the cell, forming a Ca^{2+}/CaM complex that binds to and activates nNOS [90]. The •NO radical that is produced in turn activates soluble guanylate cyclase in the postsynaptic neuron and potentially in the presynaptic neuron.

Similar to the activation mechanism found in the neuronal cells, chemical messengers (e.g., hormones or acetylcholine) bind to their corresponding receptors on endothelial cell membrane. This binding triggers the opening on a membrane channel, resulting in a flow of calcium into the cell. Once in the cell, the calcium binds to a calmodulin molecule, forming the Ca^{2+}/CaM complex that in turn activates eNOS through binding. As eNOS is bound to the inner surface of plasma membrane of the cell, the •NO produced diffuses freely into both the blood vessel and into the underlying vascular smooth muscles cells. In the blood vessel, •NO enters blood platelets and decreases their aggregation with each other and their adhesion to endothelial cells [90]. Within the muscle cells, •NO activates sGC, producing an increase in cyclic guanine monophosphate (cGMP) levels. cGMP decreases the amount of free calcium levels in the muscle cell, allowing the blood vessels to vasodilate [90].

Unlike nNOS and eNOS, inducible NOS does not require calcium for activation. Instead, the enzyme is synthesized in macrophages in response to cytokines. Once

synthesized, iNOS immediately begins production of •NO that diffuses at least partially into the nearby tumor cell. Once inside the cell, •NO can disrupt a number of cellular processes, including electron transport needed for adenosine triphosphate synthesis, and the tricarboxylic acid cycle. In addition, •NO can also inhibit the ribonucleotide reductase necessary for DNA synthesis and cell division [90].

4.3.3 The Molecular Structure of NOS

The recent advances in NOS structure analysis have shed light on the roles of the pterin, the substrate, and the newly discovered zinc ion in dimer formation and stabilization as well as catalytic activity. Work by numerous groups on iNOS (murine and human) [100, 101, 105–107], and eNOS (human and bovine) [101, 102] provides an intimate view of the various interactions between cofactors and protein–protein interplay in dimer formation. Structural work on the neuronal isoform of NOS is presently ongoing, with preliminary results indicating high structural similarity to published structures of the other NOS isoforms (T.L. Poulos, personal communication).

Prior to the elucidation of these structures, it was known that NOS must dimerize through the oxygenase domain for catalytic function [99]. Structures of the oxygenase dimer of both iNOS and eNOS reveal that dimer formation reinforces the substrate binding channel and sequesters two pterin molecules within two symmetry-related lariats (see Figure 11) [100–102]. The dimer interface is extensive with between 1200 and 2800 Å^2 of buried surface [100–102]. Additionally, conformational changes upon dimerization of iNOS expose the heme edge opposite of the center channel, and provide a possible interaction surface for the complementarily shaped reductase domain [100].

Similar to the P450s, the substrate (L-Arg) is held in place by hydrogen-bonding interactions that position the atom to be hydroxylated within 4 to 5 Å from the heme iron (Figure 12) [100–102]. Interactions of the L-Arg guanidinium group at the bottom of the heme pocket suggest a mechanism for •NO synthesis where the proton donation from the substrate to the iron-bound dioxygen facilitates heterolytic cleavage of the O–O bond, yielding Compound I [100]. This interaction serves to neutralize the guanidinium group, and discriminates between Compound I and the ferric superoxy species in the two steps of •NO synthesis. The only major difference between the binding modes of L-Arg and NHA in the active site results from the addition of the NHA hydroxyl group. The structure of this complex shows the oxime nitrogen (N^{ω}) of NHA projecting towards the center of the porphyrin macrocycle ~4 Å away from the iron [106]. This positioning leaves no proton readily available for the breakdown of the ferric superoxy complex to Compound I, thereby allowing the dioxygen species to serve as the active oxygen intermediate in the reaction of NOS with NHA. However, direct interaction between the ferric superoxy complex and NHA is unlikely. Modeling studies with the structure of NHA-bound iNOS indicate that the terminal oxygen of the ferric superoxy species is distant from the NHA hydroxyl group and therefore does not appear able to interact with this substrate moiety [106]. Instead, free radical addition of the ferric superoxy to the

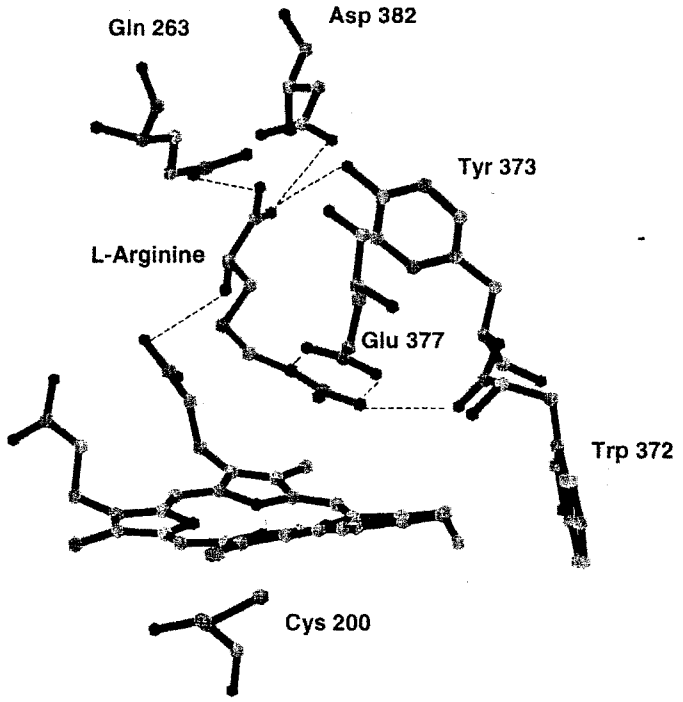

Figure 12. Key catalytic residues and the location of L-arginine in the heme active site [100]. The heme is ligated to a cysteine residue with the sixth position vacant. Dashed lines represent hydrogen-bonding interactions between the substrate and the distal heme environment as depicted in Ref. [100].

NHA oxime or proton donation from protonated N^{ω} to the heme species are suggested as likely mechanistic pathways [106]. Regardless of the final mechanism, the L-Arg and NHA-bound structures of NOS imply that NOS catalysis selects between two different reductive activations of dioxygen.

The essential pterin cofactors of the NOS bind at the dimer interface ~13 Å apart and ~40° from coplanarity (Figure 11) [100–102, 106, 107]. The H_4B heteroatoms participate in a number of hydrogen-bonding interactions—most importantly with a tryptophan residue from the same subunit, and a phenylalanine residue from the adjacent subunit (Figure 13). These two residues maintain π-stacking interactions with the H_4B pteridine ring increasing both pterin affinity and •NO synthesis activity [100–102, 106, 107]. Additionally, the pterin interacts with the same heme propionate group as L-Arg and NHA (Figure 13), allowing allosteric interaction between the pterin and the substrate via the propionate group. Recent structural

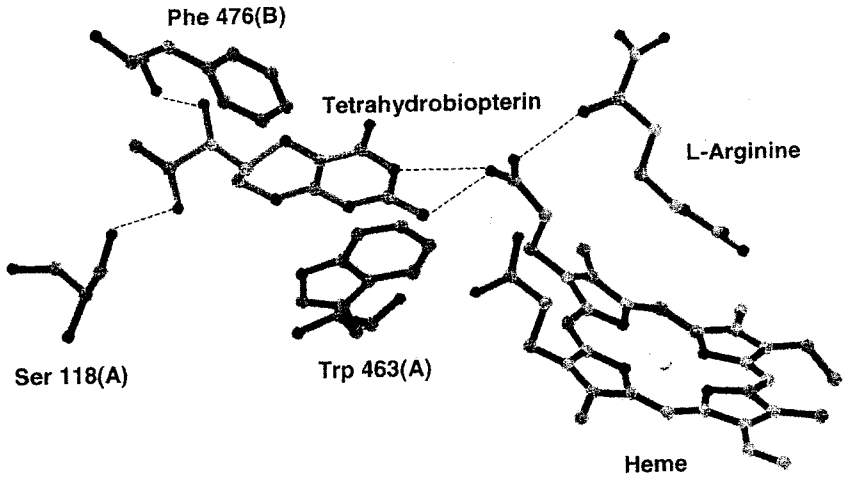

Figure 13. The H_4B binding-site in iNOS generated from the X-ray coordinates [100]. The amino acids involved in hydrogen-bonding interaction with the pterin are shown. (A) or (B) denote the subunit of the residue.

data of NOS with H_4B bound, as well as other substituted and oxidized pterins, indicates that H_4B likely binds in its neutral form and fulfills roles ranging from dimer stabilization to acting as a redox cofactor or modifier of heme reactivity [106].

The most recent discovery revealed by structural NOS data is the positioning of a tetrahedrally coordinated zinc ion at the base of the dimer interface (see Figure 11). Seen first for eNOS [102], this divalent metal site has since been observed in iNOS [100, 101, 106] and nNOS (T.L. Poulos, personal communication). The zinc ion is coordinated to pairs of symmetry-related cysteine residues, and is equidistant from both pterin cofactors (~12 Å) and heme groups (~20 Å). This remote location from the catalytic heme iron, as well as its complete coordination by four cysteines (Figure 14A), is consistent with a structural rather than enzymatic role for the zinc ion. Structures of zinc-free iNOS show the formation of a self-symmetric disulfide bond (Figure 14B) across the dimer interface that adversely effects subunit association, formation of the pterin-binding site, and catalytic activity [107, 108], supporting the structural role proposed for the zinc site. In addition, the surface of the area closest to the zinc site in eNOS is the most electropositive region of the molecular surface, and provides an excellent docking site for the strongly electronegative reductase domain [102]. Similar calculations for iNOS reveal no such surface near the zinc site, and point instead to the surface surrounding the exposed heme edge as the potential site for reductase binding [108].

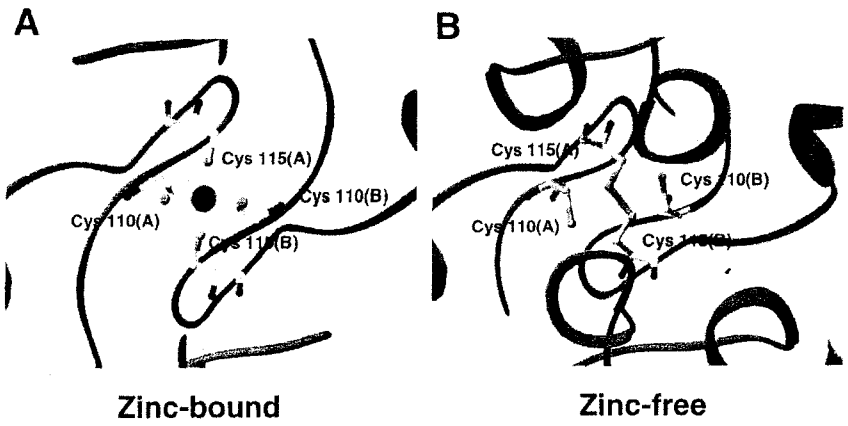

Figure 14. Ribbon drawing of the (A) zinc-bound and (B) zinc-free states of the iNOS oxygenase domain as determined by X-ray coordinates [107].

4.3.4 The Mechanism of NOS

Proposals regarding the NOS catalytic mechanism of the conversion of L-Arg to L-citrulline and •NO have ranged from sole participation of the heme cofactor (a P450-type mechanism) to interactions between the substrate, heme, and the H_4B cofactor. The conversion of L-Arg to NHA is a two-electron oxidation of one of the guanidino nitrogens of L-Arg. This step is believed to parallel a P450 hydroxylation reaction with direct involvement of the heme in oxygen activation [4, 6, 109]. In the second half of the overall reaction, the conversion of NHA to L-citrulline and •NO is a three-electron oxidation of the substrate involving electron removal, oxygen insertion, and carbon–nitrogen bond scission to form product [12, 90, 110]. NADPH stoichiometry for all three isoforms under multiple turnover conditions suggests that 1.5 mol of NADPH is consumed to generate 1 mol of •NO and L-citrulline [111–113]. Of these three electrons, the conversion of L-Arg to NHA utilizes two electrons, while the formation of •NO and L-citrulline from NHA requires the remaining 0.5 mol of NADPH. Related $^{18}O_2$ experiments demonstrated that the oxygen atoms incorporated into •NO and L-citrulline originate from different molecules of molecular oxygen [114, 115]. The interesting aspect of NOS chemistry is that the enzyme converts substrates (L-Arg, O_2 and NADPH) with an even number of electrons into products that also contain an even number of electrons (L-citrulline, water, and $NADP^+$) plus the free-radical species, •NO [90].

Conversion of L-Arg to N^{ω}-hydroxy-L-arginine

The first half of the working mechanism shown in Figure 15 originates from proposals in the NOS literature [116, 117] involving the formation of a high-valent oxo

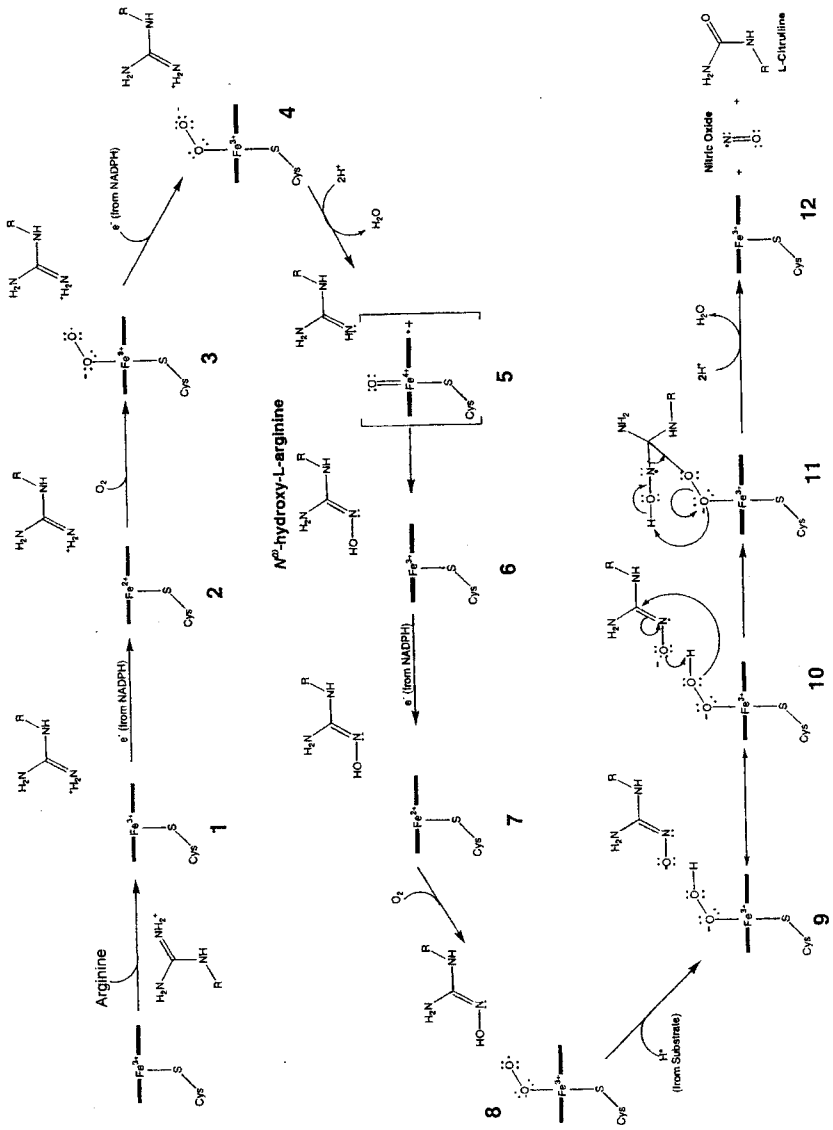

Figure 15. Proposed mechanism for the biosynthesis of nitric oxide from L-arginine. See text for details. (Adapted from Ref. [90].)

heme complex analogous to Compound I in P450 and peroxidase chemistry. Initially, the ferric five-coordinate largely high-spin resting state binds L-Arg to form the totally high-spin substrate bound complex (**1**). Upon addition of an electron from NADPH, the ferric-iron is reduced to the deoxyferrous complex (**2**). One equivalent of dioxygen binds to the ferrous heme iron to form the oxyferrous complex, shown in Figure 15 as the ferric superoxide resonance form (**3**). Addition of a second electron to **3** from NADPH is proposed to give a ferric peroxide complex (**4**) that can then be doubly protonated to lose water and yield the oxo-ferryl ($O{=}Fe^{IV}$) porphyrin radical intermediate (**5**). Unlike P450s where protons are shuttled in from the surface of the protein via a distal charge relay, structural data implicate the proton-rich guanidinium group of L-Arg as the proton source (Figure 16) [100]. The position of the terminal nitrogen 3.8 Å from the heme iron permits the donation of protons to the peroxo-iron, facilitating O–O bond cleavage and reduction of the guanidinium charge [100]. Following O–O bond cleavage, the substrate can then react with the remaining electrophilic oxo-iron species to form the hydroxylated product, NHA.

Similarities between NOS and P450 (e.g., thiolate-ligation to the heme, close proximity of the substrate to the active oxygen intermediate, and O_2 and NADPH requirements) provide a powerful argument for a P450-type reaction mechanism. However, other mechanistic proposals have been offered which liken NOS to an amino acid hydroxylase rather than to a P450. The reasoning behind an alternative catalytic pathway for NOS is two-pronged. First, hydrogen peroxide is unable to catalyze the formation of NHA from L-Arg. This reaction—also known as the peroxide shunt—allows hydrogen peroxide to replace O_2 and the two electrons from NADPH, and is well established for P450 enzymes. Second, experiments by Perry and Marletta determined that addition of exogenous nonheme iron increased nNOS activity [118]. This stimulation led to the proposal that the pterin and the nonheme iron are in close proximity such that both participate in oxygen activation and hydroxylation [118]. This catalytic mechanism would account for the inability of hydrogen peroxide to substitute for oxygen and NADPH. Recent crystallographic analysis of tyrosine hydroxylase [119] and NOS [100–102, 106] refute these proposed roles for mononuclear iron and the pterin by revealing little similarity between the two enzymes. In fact, no mononuclear metal binding site could be found in NOS [100–102, 106]. In light of this evidence, the monooxygenation of L-Arg by NOS likely follows a P450-type mechanism, despite the ineffectiveness of hydrogen peroxide in catalytic turnover.

Conversion of N^{ω}-hydroxy-L-arginine to L-citrulline and •NO

Single turnover experiments by Stuehr and coworkers have determined that only one exogenous electron is necessary for conversion of NHA to products [120]. These results argue against participation of the P450-like oxo-ferryl intermediate and instead favor a ferric-superoxide complex as the reactive oxygen intermediate in the catalytic mechanism. In the first half of the NOS reaction, the ferric superoxy complex is thought to be only an intermediate that leads to a "reactive oxygen species" capable of hydroxylating L-Arg, whereas in the second half it may react

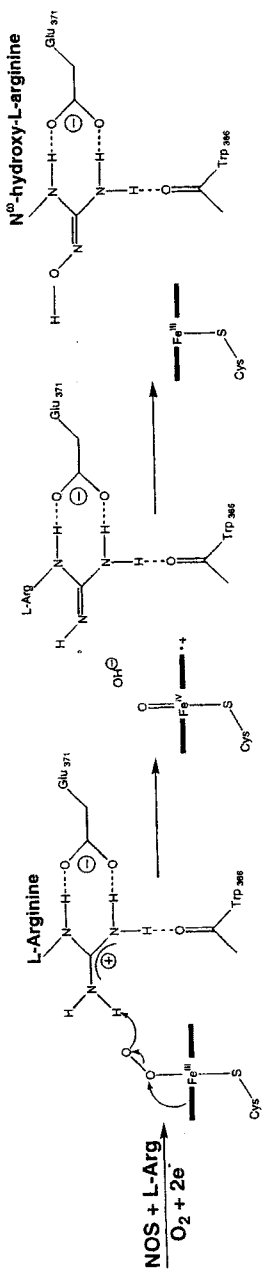

Figure 16. Proposed L-arginine-assisted NOS oxygen activation. First, substrate L-arginine (only guanidinium shown) donates a proton to the peroxo-iron, facilitating O–O band cleavage and conversion to a proposed oxo-ferryl π-cation radical species. The radical species then rapidly hydroxylates the neutral guanidinium to N^{ω}-hydroxy-L-arginine. (Adapted from Ref. [100].)

directly with the substrate, NHA. Following the formation of NHA (Figure 15), reduction of the regenerated ferric five-coordinate species (**6**) by an electron from NADPH yields a five-coordinate ferrous adduct (**7**). Dioxygen binds in the sixth coordination site to form the ferric-superoxide complex (**8**). A hydrogen atom from the NHA reduces the ferric-superoxide adduct to form the ferric-hydroperoxide complex (**9**) and a cation radical on the guanidino carbon of the substrate. The ferric-hydroperoxide species nucleophically attacks the guanidino carbon ($^{-}O-\dot{N}^{+}=C(NH_2)-NHR$) of the substrate (**10**), which undergoes electron arrangement (**11**) to produce L-citrulline, •NO, and the ferric resting state (**12**) [12, 110].

The exact identity of the reactive oxygen intermediate in the conversion of NHA to products is the focus of much experimental investigation. Structures of NHA-bound iNOS [106] impose mechanistic constraints due to steric clash between NHA and the iron-bound dioxygen ligand. This negative interaction favors either free radical addition of the ferric superoxy to the NHA oxime or proton donation from protonated N^{ω} to the heme species [106]. Furthermore, positioning of the NHA hydroxyl group may direct NOS towards a ferric-peroxo-NHA radical intermediate prior to breakdown into products [106]. However, these structures do not discount participation of a high-valent iron-oxo species in the second half of the reaction. In fact, an iron-oxo would be well situated relative to the NHA oxime to form an oxaziridine (which has a triangular ring with C, N, and O atoms) that could ring-open to produce L-citrulline and •NO [106]. This type of intermediate has also been proposed to explain the additional products, cyanoornithine and NO^{-}, observed when the NOS reaction is shunted with peroxide [121]. However, L-citrulline formation in the hydrogen peroxide-dependent oxidation of NHA can be accounted by either mechanism involving a ferric peroxo or an iron-oxo intermediate. Thus, the reaction with hydrogen peroxide cannot be considered to occur exclusively via an iron-oxo intermediate. The lack of cyanoornithine and NO^{-} under natural turnover conditions favors ferric superoxy over Compound I as the reactive oxygen intermediate when NADPH and O_2 serve as reactants. Recent spectral evidence obtained by Stuehr and coworkers [114] demonstrates that the ferrous oxygenase domain of nNOS can catalyze a quantitative conversion of NHA and dioxygen to citrulline and •NO in a single turnover reaction. Stopped-flow spectral analysis indicates formation of a ferrous-oxy (or ferric superoxy) species ($\lambda_{max} = 427$ nm) prior to NHA oxidation [116]. Two other groups, using full-length NOS with bound L-Arg [122] or nNOS oxygenase domain with bound N^{ω}-methyl-L-Arg [123], have observed a ferrous-oxy species that exhibits a considerably more blue-shifted Soret absorption band ($\lambda_{max} = 415$–419 nm) at $-30\,^{\circ}C$ in 50 % ethylene glycol. Examination of the formation and reactivity of the ferric superoxy complex with NHA shows a build-up of the ferric NO species prior to regeneration of the ferric resting state [116]. The accumulation of this intermediate establishes the •NO radical as the primary product rather than other N-oxides such as nitroxyl, which would generate a ferrous NO complex with the heme. The sum of these studies, while not completely dismissing Compound I as an active participant in catalytic turnover, supports the proposed mechanism shown in Figure 15, indicating that the O–O bond is intact during the NHA oxidation in NADPH-dependent catalysis.

The role of tetrahydrobiopterin

Initially, the role of H_4B in the NOS system appeared to one of dimer stabilization, as indicated by its tight binding at the dimer interface [100–102]. Recent structural and mechanistic investigations have helped to clarify and expand this role, arguing that the cofactor may also participate directly in the NOS catalytic mechanism. Comparison of a series of dihydro- (H_2B) and tetrahydropterins (H_4B) in supporting electron transfer, •NO formation, and dimer formation demonstrates the absolute requirement for reduced pterin for formation of products but not for stable dimer formation [124]. In addition, H_4B decreases the stability of the NOS oxyferrous complex [125], which clearly implies communication between the pterin and heme sites. Studies of dimerization and catalytic competency of H_4B-free iNOS indicate that the pterin is essential for conversion of L-Arg to NHA, but not for conversion of NHA to products [104]. The inability of pterin-free NOS to convert L-Arg to NHA implies a direct catalytic role for H_4B in this portion of the reaction mechanism. Low-temperature, rapid-reaction experiments investigating the effect of H_4B on the decay of the oxyferrous complex of nNOS indicate that the pterin donates an electron to the heme dioxy complex in the presence of L-Arg [122]. Furthermore, recent EPR experiments show the formation of an apparently stable H_3B• radical under single turnover conditions when L-Arg is the substrate [117]. These results, coupled with the known location of the pterin within the crystal structure, are most consistent with H_4B being involved in electron transfer to the heme group in NOS rather than direct interaction with the substrate. The role of H_4B in the conversion of NHA to products is more ambiguous. Pterin-free NOS is still able to convert NHA to L-citrulline and •NO; however, cyanoornithine and NO^{-} are also formed [104]. The variation of the product profile in the absence of H_4B implies a role for the pterin in the NHA reaction. A direct redox role is unlikely, as some L-citrulline and •NO are formed. However, the formation of the cyanoornithine and NO^{-} products is similar to the effect of shunting NOS with peroxide, indicating that the pterin may play a role in the modulation of the reductive pathway of the ferric superoxy heme complex.

4.4 Heme-Containing Plant Peroxidases

4.4.1 Introduction

Heme peroxidases are found extensively throughout the plant, animal, and bacterial kingdoms. These enzymes catalyze the oxidation of a wide variety of organic and inorganic substrates, with the concomitant reduction of hydrogen peroxide or other hydroperoxides (ROOH) to water to alcohols (ROH), respectively:

$$H_2O_2 + 2AH \rightarrow 2H_2O + 2A$$

Peroxidases fall into two superfamilies (plant and mammalian) and a third, indistinct group that includes chloroperoxidase (a P450-like hybrid) and di-heme cytochrome *c* peroxidase from *Pseudomonas aeruginosa*. The plant peroxidase superfamily contains enzymes of plant, fungal, and bacterial origin [126]. Mammalian peroxidases make up the second superfamily, and include lactoperoxidase, myeloperoxidase, and prostaglandin H synthase. Both families have been the focus of numerous excellent reviews, several of which have discussed the differences between the plant and mammalian peroxidases [126–130]. Here, recent experimental investigations focused on the plant peroxidases will be discussed.

The plant peroxidase superfamily can be further divided into three classes based on sequence and structural similarities [126]. Class I constitutes intracellular peroxidases of prokaryotic origin, such as yeast cytochrome *c* peroxidase (CCP) and pea cytosolic ascorbate peroxidase (APX). The main role of this class of peroxidases appears to be the removal of hydrogen peroxide. Secretory fungal peroxidases such as lignin peroxidase (LIP) and manganese peroxidase (MnP) from *Phanerochate chrysosporium* and *Corpinus* peroxidase (CIP) make up Class II. These enzymes are monomeric glycoproteins, with four conserved disulfide bridges and two conserved calcium sites. The secretory plant peroxidases form Class III. These enzymes are also monomeric glycoproteins, with four conserved disulfide bridges and two conserved calcium sites; however, the location of the disulfide bridges varies from those in Class II enzymes. Enzymes in Class III include peanut peroxidase (PNP), barley grain peroxidase (BP 1), and horseradish peroxidase (HRP), the most thoroughly investigated heme-containing peroxidase.

4.4.2 The Molecular Structure of Heme Peroxidases

In 1980, CCP became the first heme peroxidase to be structurally characterized. Reaction mechanisms, substrate binding sites and ligand interactions were proposed based on the various structures of CCP and carefully applied to the entire plant peroxidase family. During the past decade, a vast number of X-ray crystal structures have been reported for other members of the plant peroxidase superfamily. Presently, structural data are available for members of Class I: CCP [131–137] and APX [138–140]; Class II: MnP [141, 142], LIP [143, 144] and CIP [145]; and Class III: HRP [146–148], PNP [149] and BP 1 [150]. Of the numerous plant peroxidases, Class III members are the most readily available and have been the most extensively studied. The solution of crystal structures of three Class III peroxidases is a recent and exciting development. These structures provide researchers with the structural framework for addressing several mechanistic questions, such as how and where substrates bind to the enzyme, and how the protein controls the location of oxidizing equivalents derived from peroxide. In addition, the availability of structural information for the members of each class gives researchers the first opportunity to compare closely the tertiary environment among members of the same and different classes. This comparative power provides great insight into the relationship between structure and function within the plant peroxidase superfamily.

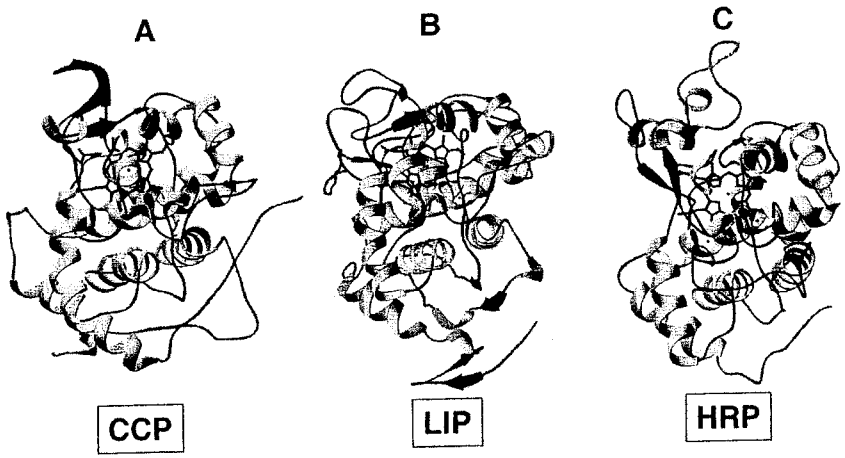

Figure 17. Schematic representation of the secondary structure of (A) CCP; (B) LIP; and (C) HRP determined from X-ray coordinates [137, 143, 211]. Helical regions, β-sheet regions, and the heme group are shown.

Although there is little sequence homology (often <20 %) within the plant superfamily, the overall folding and organization of the secondary structure is conserved. Figure 17 shows a side-by-side comparison of the secondary and tertiary structure of a representative member of each plant superfamily class. The enzymes are divided into N- and C-terminal domains, with the heme positioned in a cavity at the domain interface. The secondary structure is dominated by α helices (10 to 11 helices) connected by loops and turns of varying lengths. β-sheet structure is minimal. There are nine invariant residues in the plant peroxidase superfamily, five of which are involved in catalysis [128]. The other conserved residues play important structural roles, such as a buried salt bridge between an aspartate and arginine and several glycine and proline residues that direct the orientation of the peptide backbone [126, 129]. Figure 18 shows the active site environment of CCP, LIP, and HRP and the nonvariant residues. The proximal ligand to the heme is a histidine residue that is anionic in nature due to a conserved hydrogen bond to a proximal aspartate residue [128]. On the distal side of the heme, a polar histidine and arginine couple form a hydrophobic cavity above the heme that is important in the stabilization of the bound peroxide and the heterolytic cleavage of the O–O bond [128]. Additionally, an aromatic tryptophan (Class I) or phenylalanine (Class II and III) on the distal side of the heme helps to stabilize the high-valent oxygen intermediates as well as to exclude substrates from the active site. Similarly, a tryptophan (Class I) or phenylalanine (Class II and III) can be found in the proximal cavity and is believed to direct the location of the second oxidizing equivalent of Compound I [128].

In addition to these similarities, there are several distinctions among the plant peroxidases that help to differentiate between catalytic mechanism and substrate

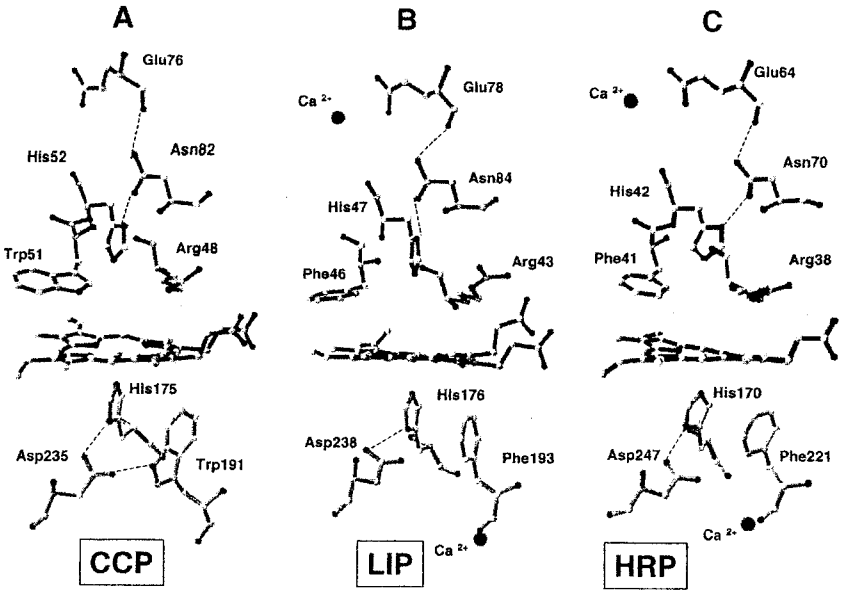

Figure 18. Key catalytic residues for (A) CCP; (B) LIP; and (C) HRP determined from X-ray coordinates [137, 143, 211]. The heme group is coordinated by a histidine and the sixth position is vacant. Calcium-binding sites for LIP and HRP are shown as spheres. Dashed lines represent hydrogen-bonding interactions.

affinity of the class members. In Class II and III peroxidases, all the cysteine residues in the protein (8 to 10 residues) form disulfide bridges that impart a high degree of rigidity to the protein [129]. Glycosylation sites for the Class II and III peroxidases point away from the molecule and are evenly distributed over the surface of the protein. This scattering suggests that the purpose of the carbohydrates is to increase the solubility of the enzyme in water, and perhaps to increase resistance to free radical-induced protein cross-linking [146].

With the exception of CCP, it is widely accepted that substrates interact with peroxidases at the heme edge rather than above the heme, as seen for the oxygenases. This postulation has been supported by structural and chemical modification data. Chemical modification studies with HRP have shown that the area directly above the heme is inaccessible to exogenous substrates [151–153]. Instead, suicide inhibitors bind at the δ-meso heme carbon (see Figure 1). The structure of HRP in the presence of benzhyroxamic acid (BHA), a model for oxidizing substrates, demonstrates that the aromatic portion of BHA does in fact interact with the proposed aromatic binding region of HRP located at the heme edge [147]. However, BHA is an atypical reducing substrate with unique hydrogen bonding potential for the

active site residues of the distal heme pocket, and therefore may not be an accurate structural model of the peroxidase–substrate complex. Recently, a structure of the HRP–ferulic acid (FA) complex in the presence and absence of cyanide has been published [148]. As FA is known to act as an in vivo substrate for peroxidases [148], these structures may provide a more precise model for the oxidation of small phenolic complexes by a plant peroxidase. Similar to BHA, FA binds in the aromatic binding pocket, but its exact orientation is ambiguous due to a flexibility of the aromatic donor binding region. This flexibility allows for the fast exchange of solvent molecules and small phenolic compounds, thereby protecting the heme group from autooxidative damage by the radical product of catalytic turnover [148]. Addition of cyanide to the system yields a six-coordinate low-spin heme complex that is thought structurally to model the transient intermediate (Fe^{3+}–OOH^-) prior to Compound I formation. Comparison of the structures of this ternary complex (HRP–FA–CN) with those of native HRP, the HRP–BHA and the HRP–FA species illustrates movement of the distal histidine 0.5 Å towards the cyanide nitrogen, thus supplying a short hydrogen bond to stabilize the binding of the ligand. The distal arginine does not move in any of the structures, but does help to stabilize cyanide by forming a hydrogen bond to the cyanide nitrogen [148]. This stabilization role for the distal arginine may imply that the residue assists in heterolytic bond cleavage by acting as a hydrogen bond donor to the transient Fe^{3+}–OOH^- complex [148]. Similar to HRP, both APX and MnP have been shown to interact with their respective substrates at the heme edge rather than above the prosthetic group [139, 141, 142].

As the peroxidases interact with their substrates via the heme edge, it is important that the oxidizing equivalents of the high-valent active oxygen intermediates are accessible to the substrates. To this end, two calcium-binding sites—one distal and one proximal to the heme—serve dual structural and catalytic roles for the Class II and III proteins [127–129]. The distal site is important in the ordering of the distal active site residues, particularly the catalytically active histidine [127]. The proximal cation is responsible for structural stability, as well as promoting the location of the second oxidizing equivalent on the porphyrin macrocycle rather than a protein residue [127]. APX, a Class I peroxidase, contains a single cation binding site on the proximal side of the heme occupied by a potassium ion [138]. The cation destabilizes the electrostatic environment surrounding the proximal tryptophan involved in hydrogen bonding interactions with the proximal histidine ligand and the nearby aspartate (Figure 19). This long-range electrostatic effect forces the second oxidizing equivalent of Compound I to remain on the heme macrocycle, ideally positioned for reactions at the heme edge [154]. CCP, also a Class I peroxidase, interacts with its natural substrate, cytochrome *c*, not at the heme edge but via an electron transfer pathway that begins at Trp191 and terminates at the protein surface (Figure 20). As a result, CCP has no bound cations and maintains a stable cation radical on the indole ring of Trp191 rather than the porphyrin during catalytic turnover [137]. The continuing accumulation of structural information for plant peroxidases will allow the key similarities and differences to be exploited through mutagenesis to explore the physiochemical differences between members of the plant superfamily.

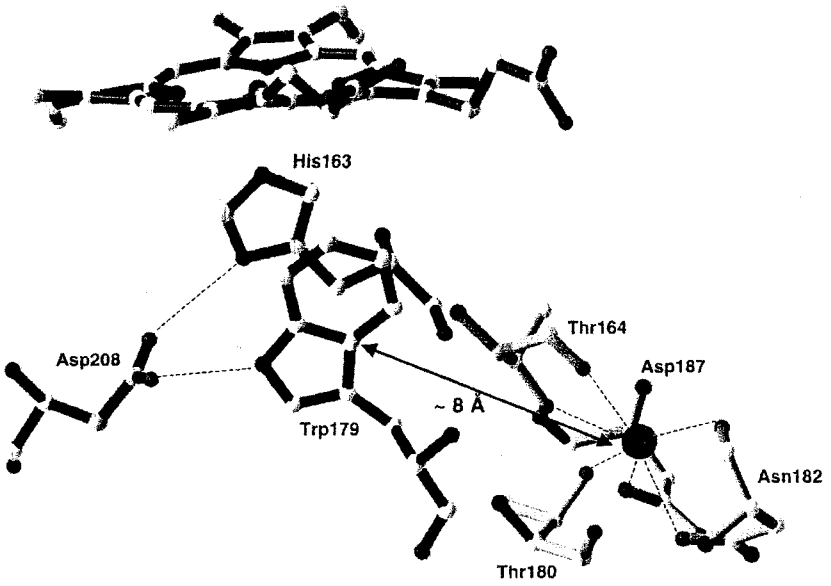

Figure 19. The APX proximal residues and cation-binding pocket generated from the X-ray coordinates [139]. The cation is shown as a sphere, with its protein interactions represented by dashed lines.

4.4.3 The Catalytic Mechanism of Heme Peroxidases

The general peroxidase mechanism

Following the determination of the crystal structure of CCP, a catalytic mechanism for its reaction with hydrogen peroxide was proposed [131, 136]. Due to the conservation of the active site residues in the plant peroxidase superfamily, similar mechanisms of Compound I formation are also thought to hold for other plant and fungal peroxidases. Of the structures shown schematically in Figure 21, three have been spectroscopically, and structurally characterized while two are proposed intermediates. The pathway is initiated by the direct reaction of neutral hydroperoxides (ROOH) or hydrogen peroxide with the ferric five-coordinate high-spin resting state complex (**1**) to generate a transient hydroperoxide adduct termed Compound 0 (**2**). Formation of this intermediate species is postulated by theoretical molecular dynamic simulations [155] and density functional studies [156], as well as being observed for HRP at low temperature [157]. This intermediate species then undergoes a protein-assisted conversion to an oxywater complex (**3**) [155, 156]. Facile heterolytic O–O bond cleavage of this oxywater complex yields the high-valent active oxygen intermediate, Compound I (**4**). For the majority of peroxidases

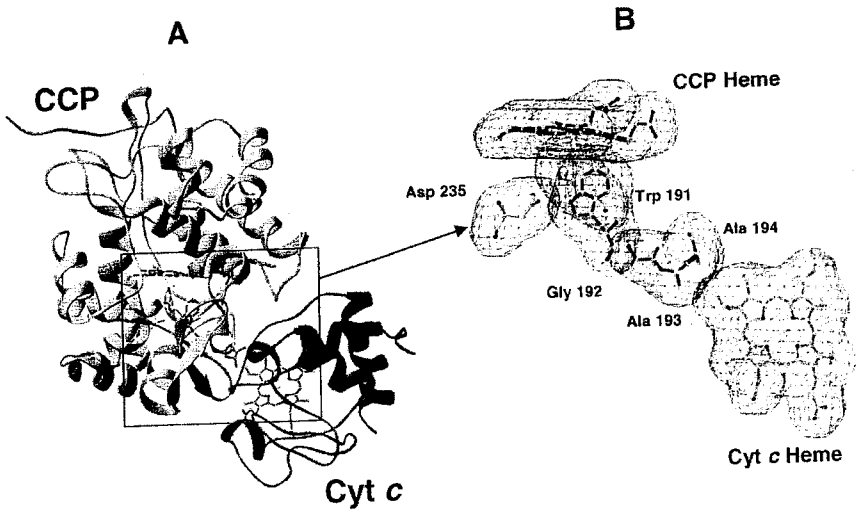

Figure 20. (A) Ribbon drawing of the interaction between CCP and its redox substrate, cytochrome *c* determined from X-ray coordinates [137]. The hemes are shown for CCP and cytochrome *c* along with the proximal residues involved in electron transport between the proteins. (B) A close-up of the electron transport chain and their overlapping electron density.

this complex is an oxo-ferryl species with a porphyrin cation radical similar to the Compound I seen in the P450 catalytic cycle (see Figure 4, complex 7). In CCP, the second oxidizing equivalent is intramolecularly transferred from the porphyrin to proximal Trp191 residue (Figure 18A), yielding a stable complex with a protein cation radical coupled with an oxo-ferryl heme [158, 159]. Reduction of Compound I to Compound II (**5**), an oxo-ferryl complex, and then to the ferric resting state, occurs with concomitant one-electron substrate oxidation forming reactive transient radical species that may dimerize, disproportionate, or attack another species causing cooxidation. Alternatively, oxygen atom donors can be added to the ferric resting state to generate Compound I, via a shunt pathway similar to that seen for P450 enzymes.

Influence of the active site environment on heme coordination and reactivity

The distal cavity

Extensive crystallographic and mutagenic studies have identified the key catalytic residues important in the formation and stabilization of the active oxygen intermediates. On the distal side of the heme, the conserved distal arginine/histidine couple is vital to efficient catalytic turnover by stabilizing and heterolytically cleaving bound peroxide to form the high-valent intermediate, Compound I (see Figure 7) [128]. The distal histidine acts as a general acid–base catalyst in the reaction of a

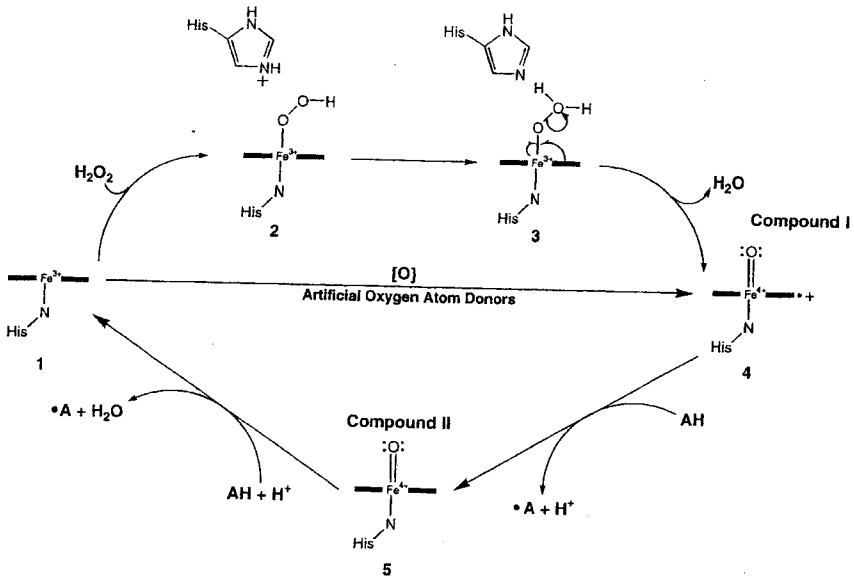

Figure 21. Peroxidase reaction cycle. AH represents the oxidizable substrate, and •A is the product. See text for details.

peroxidase with hydrogen peroxide by first deprotonating the iron-bound oxygen of peroxide (Figure 21, **2**) then transferring the proton to the outer oxygen (Figure 21, **3**) [128]. Deletion of this residue in both CCP (H52L) and HRP (H42A and H42V) results in the drastic reduction of the rate of Compound I formation by five orders of magnitude [160, 161]. This decrease in activity is presumably due to the elimination of a critical acid–base catalyst from the active site. Interestingly, activity of the H42A HRP mutant is restored by the addition of exogenous 2-substituted imidazoles (H42A + imidazole) [162]. Bronstead analysis predicts that ~60 % of a positive charge develops on the imidazole in the transition state of Compound I formation [162], confirming the acid–base role of the distal histidine.

Surprisingly, conversion of His42 of HRP to a glutamate [163], a residue shown to participate in general acid–base chemistry in chloroperoxidase (CPO) [164], yields an enzyme with lowered rates of Compound I formation and lowered levels or peroxidase activity [163]. In CPO, Compound I is formed at a rate (2.3×10^6 M^{-1} s^{-1}) [165] much higher that H42E HRP (4.9×10^3 M^{-1} s^{-1}) and comparable to wild-type HRP (1.4×10^7 M^{-1} s^{-1}) [163]. The inefficient formation of Compound I is likely due to a decrease in the basicity of the glutamate residue and its improper orientation in H42E HRP compared to that of the native histidine. These alterations in the distal pocket destabilize the heme-peroxide-Glu42 ternary intermediate of the peroxide reaction [163]. The crystal structure of CPO shows that the distal

Glu is fixed in position by a hydrogen bond with an adjacent histidine [164]. Similarly, the orientation and basicity of the distal histidine in the plant peroxidases appears to be maintained by conserved hydrogen bonding interactions between the catalytic histidine and a highly conserved asparagine residue (see Figure 18). In HRP, mutation of this asparagine (Asn70) to valine (N70V) abolishes its hydrogen-bonding capabilities, causing a decrease in the rate of Compound I formation [166, 167]. Further studies reveal that its replacement with an aspartate (N70D) yields a mutant that should maintain the hydrogen bond with His42 but is still inactive [168]. Inactivation of HRP is likely due to the loss of a second hydrogen bonding interaction between Asp70 and the backbone carbonyl of a conserved glutamate residue (Glu64; Figure 18C). The disruption of this secondary interaction alters the orientation of the aspartate with regard to His42, resulting in the breakage of the Asp70–His42 hydrogen bond [168]. These findings demonstrate the manner by which the active site environment of the plant peroxidases has evolved to stabilize and promote the distal histidine as an active participant in the formation and stabilization of Compound I.

In contrast, the distal arginine residue does not appear to be absolutely essential in the formation of Compound I. In the mechanism proposed by Poulos et al. [131], the positively charged distal arginine is responsible for the promotion of O–O bond heterolysis by stabilizing the precursor enzyme–peroxide complex. Consistent with this proposed role, mutation of this polar residue to a neutral leucine in HRP (R38L) and CCP (R48L) causes a decrease in the rate of Compound I formation, particularly in the HRP mutants [169–173]. The reasoning for this variation of mutagenic effect stems from the increased polarity of the CCP distal pocket compared to that of HRP. As a result, the deletion of the distal arginine in CCP does not cause as drastic an effect on the ability of the enzyme to form Compound I [170, 171]. Moreover, the recently demonstrated crystal structure of HRP with ferulic acid and cyanide bound indicates that the distal arginine does indeed stabilize the bound ligand through hydrogen-bonding interactions [148].

Additional experiments with R38L HRP indicate that Arg38 may also play an important role in the binding of peroxide to the heme iron [171]. Researchers propose that the polar character of Arg38 in HRP facilitates the access of hydrogen peroxide to the heme and/or provides an electrostatic interaction with the incoming peroxide, which may induce the deprotonation of hydrogen peroxide at neutral pH [171]. Additionally, the reaction of H38L HRP with hydrogen peroxide results in the accumulation of a previously unseen intermediate formed prior to Compound I formation [171]. The spectroscopic properties of this complex are dissimilar from those of the proposed ferric peroxy intermediate (Figure 21, **2**) isolated at low temperature for the reaction of wild-type HRP with peroxide [157]. Theoretical molecular modeling studies assign the new spectral intermediate to a neutral peroxide-bound ferric heme species [174].

In both peroxidases, the decay of Compound I is drastically increased by the deletion of the distal arginine, emphasizing its role as a stabilizer of the high-valent intermediate [169–171, 173, 175]. Crystallographic and resonance Raman data have shown that the distal arginine is very flexible, and can move towards or away from the ligand in the sixth position as needed [135, 176]. This flexibility allows the gua-

nidinium groups to move inside the cavity and form a stabilizing hydrogen bond with the ferryl oxygen atom of Compound I and II [134].

The proximal cavity

Crystal structure data from representatives of each of the three classes of the plant peroxidase superfamily confirm that the side chain of an aspartate residue is involved in a key hydrogen bond to the Nδ1H of the proximal histidine residue (see Figure 18) [128, 146]. The purpose of this residue has been most investigated for CCP where the carboxylate side chain of Asp235 is involved in hydrogen bonds with both Trp191 and the proximal His175 ligand (Figure 18A). Using the wild-type enzyme and three CCP mutants (D235A, D235E, and D235N), three main roles have been proposed for this residue based on extensive spectroscopic characterization [71, 177]. First, the strong hydrogen bond from the proximal His to the adjacent Asp is believed to increase the electron density on the histidine imidazole ring, which in turn allows the imidazole group to stabilize the heme iron as it cycles through ferric and ferryl states during the catalytic cycle [71, 177]. Second, the strong hydrogen bond is believed to hold the iron below the heme plane, helping to maintain a vacant sixth coordination site [178]. Finally, the formation of a second hydrogen bond with the catalytically important Trp191 optimizes the orientation of the Trp side chain with respect to the heme and His175. Interestingly, the D235N CCP only showed a five-fold decrease in the rate of formation of Compound I [71] while the D235A CCP mutant rapidly forms Compound I [177]. These results demonstrate that the electronic donation to the heme iron via His175 does not significantly increase Compound I formation, indicating that Asp235 is not especially important for the reaction of the peroxidase with hydrogen peroxide. Recent mutagenic studies on CIP (D245N) and MnP (D242S and D242E) (two Class II peroxidases) confirm that changes in the axial ligand hydrogen-bonding network alter the occupancy of the sixth coordination site for the ferric protein as well as the reactivity of Compound II but not Compound I [179–181]. Similarly, mutation of the proximal ligand itself (His175) to Gln, Glu, or Cys results in CCP mutants that react with hydrogen peroxide as fast as wild-type CCP with the H175E mutant being hyperactive [182, 183]. Taken together, these data emphasize the importance of the distal rather than the proximal residues in the formation of Compound I. However, the proximal environment serves the equally significant roles of maintaining a free sixth coordination site for hydrogen peroxide binding and stabilizing Compound I once formed.

The role of the divalent cations in Class II and III peroxidases

All Class II and III plant peroxidases have two calcium binding sites, one proximal and one distal to the heme plane (see Figure 18B and C). These divalent cations appear to be vital for efficient peroxide catalysis by maintaining the structural integrity of the heme active site and directing the location of the second oxidizing equivalent derived from peroxide. A series of mutagenic studies with LIP and MnP ascertain that the calcium ions for these two peroxidases are released upon thermal inactivation [184–186]. The loss of these ions results in perturbations of the coordination sphere of the heme iron. LIP converts from an active five-coordinate high-spin complex to a mixture of active five-coordinate high-spin and inactive six-coordinate low-spin species [184]. The heme environment of MnP is particularly altered, resulting in an inactive six-coordinate low-spin complex with spectroscopic characteristics consistent with bis-histidyl ligation [185, 186]. In HRP, mutation of Glu64—a residue involved in both calcium binding and a hydrogen-bonding network with His42—gives an enzyme with significantly decreased oxidation activities [187]. This decrease in activity is attributed to the loss of the distal calcium ion, which causes the reorientation of both His42 and Arg38 [187].

APX contains a single cation binding site occupied by a potassium ion (see Figure 20) [138, 140]. This site is not seen for CCP, implicating the cation in the catalytic mechanism or regulation of APX. Similar to CCP, APX has an aromatic tryptophan on the proximal side of the heme that forms hydrogen bonds with both the proximal histidine ligand and the nearby aspartate (Figure 19) [138, 140]. In CCP, the analogous tryptophan is the location of the second oxidizing equivalent of Compound I. However, in APX, this equivalent is located on the porphyrin, similar to the Class II and III peroxidases [128, 154, 188]. Incorporation of a cation binding site into CCP results in an enzyme that is unable to form a stable cation radical on the proximal tryptophan. These results suggest that long-range electrostatic effects can control the reactivity of a redox amino acid side chain [189–191]. A similar result is seen for a mutant of HRP where the redox inactive proximal phenylalanine is replaced with a tryptophan (F221W). In this case, an unstable tryptophan cation radical is formed upon reaction with peroxide, but quickly dissipates into the protein matrix due to the improper orientation of the indole ring and its proximity to the proximal calcium ion [192]. Deletion of the cation site in APX results in an inactive six-coordinate low-spin species with spectroscopic similarity to a bis-histidyl complex [193]. Despite being located ~8 Å from the peroxide binding site, mutation of residues involved in binding of the potassium ion results in long-range conformational alterations [193]. Taken together, these studies emphasize the role the proximal cation plays in the both location of the oxidizing equivalents of Compound I, as well as in the preservation of the structural integrity of the heme active site.

4.4.4 Can Peroxidases Catalyze Peroxygenase Chemistry?

With resemblance of the active intermediates of their respective mechanistic cycles, it is somewhat surprising that peroxidase and monooxygenases do not catalyze similar reactions. Investigations by Ortiz de Montellano and coworkers have shown that the extent of protein surface exposure of the heme macrocycle for peroxidases and P450s plays an important role in the discretion of function of the enzyme [152, 153, 194]. Examination of reactions of HRP and P450CAM with alkyl- and phenylhydrazines shows that the hydrazine interacts with the iron of the monooxygenase, but is limited to the heme edge of the peroxidase [151–153]. Various distal side mutations in HRP have been made in an effort to maintain catalytic efficiency while opening up the distal cavity [162, 195]. Enhanced oxygenase activity

of HRP mutants such as F41A [161], H42A [161], H42E [163], and the two double mutants, F41H/H42A [195] and H42A/R38H [127] is the direct result of increasing substrate accessibility to the oxo-iron of Compound I. These results support the current hypothesis that the reactivity of the heme prosthetic group depends not only on the coordination of the heme iron itself but also on the topology of the protein surrounding it.

4.4.5 Development of CCP as a Protein Model System for Heme-Containing Enzymes

Complementary to the studies of native proteins and synthetic model systems, site-directed mutagenesis allows researchers rationally to design structural and catalytic mimics for different heme proteins from basic protein scaffolding such as CCP. This technique enables the researcher to alter the axial ligation of the protein in order to test principles obtained from earlier studies on the native protein, and to determine key structural features governing the discretion among protein functions. In the area of P450 models, this technique has been utilized to replace the histidine proximal ligand of CCP with a cysteine in order to engineer a P450-like protein in a peroxidase protein environment [183, 196]. Peroxidase and P450 enzymes have similar proposed reaction intermediates (e.g., Compounds I and II), though the lifetime and reactivity of those intermediates vary. As the main difference between a peroxidase and a P450 protein is the ratio of electron transfer to oxygenation, or the branching ratio, the catalytic differences between CCP and P450 are quite subtle. Initial attempts to place a cysteine ligand into a peroxidase environment were not successful [181]. Poulos and coworkers mutated the proximal His175 of CCP to Cys, but this did not result in thiolate ligation to the heme [183]. Instead, they determined by X-ray crystallography that the proximal Cys had been oxidized to cysteic acid [183]. It was suggested that this had occurred due to the smaller size of Cys relative to His, presumably leaving the Cys too far from the heme iron to bind properly, and thus susceptible to oxidation. Recent work by Lu, Dawson and coworkers indicates that the negative charge of the proximal Asp235 residue of CCP conflicts with the negative charge of the mutated thiolate ligand [196]. Replacement of Asp235 with a leucine residue resulted in a double mutant of CCP (H175C/D235L) which has UV-visible, magnetic circular dichroism and EPR spectral characteristics that are similar to those of camphor-bound P450 [196], indicating the potential of this system as a model for P450 enzymes.

Rational design has also been utilized to engineer artificial metal binding sites into CCP in an effort to mimic the active sites of MnP (a heme and manganese ion center), cytochrome *c* oxidase (COX, a heme and Cu_B center) and the potassium-binding site of APX. In the case of the MnP mimic, creation of a manganese binding site near the heme of CCP results in a model system which binds a single manganese ion, reacts with hydrogen peroxidase to form Compound I, and catalyzes the steady state oxidation of Mn^{2+} at enhanced rates compared to wild-type CCP [197–199]. In an effort to improve the MnP model, the two active site tryptophan residues (Trp191 and Trp51) of CCP have been mutated to their MnP-analogous phenylalanine residues [200]. The results of this study demonstrate that, while the W191F and W51F mutations both play important roles in stabilizing Compound I, only the W51F mutation contributes significantly to increasing the MnP activity [200]. This effect is attributed to the ability of this mutation to increase the reactivity of Compound II, whose oxidation of Mn^{2+} is the rate-determining step in the reaction mechanism [200]. Preliminary results for the COX mimic indicate the successful binding of a copper ion above the heme plane of CCP upon mutation of three distal residues to histidines (R48H, W51H, and S81H) [201]. EPR studies of this CCP mutant strongly suggest that the heme Fe(III) is antiferromagnetically coupled to the added Cu(II) similar to the case in the Cu_B-heme center in all terminal oxidases [201]. Design of a proximal cation binding site similar to that seen for APX and the Class II and III plant peroxidases has also been accomplished for CCP [190, 191]. As expected, insertion of a potassium ion on the proximal side of CCP heme increases the electrostatic potential surrounding Trp191, and the proximal environment is no longer able to effectively stabilize a cationic Trp radical [190, 191]. In an extension of this work, slight alteration of the CCP template that binds potassium results in a CCP mutant that can bind a calcium ion [189]. Similar to the potassium-bound CCP, the cation decreases the stability of the Trp191 cation radical during hydrogen peroxide turnover [189]. The engineering of these varied metal-binding sites yields a deeper understanding for the structural factors that control metal-binding site selectivity.

In a departure from designing artificial metal-binding sites within CCP, recent attention has focused on replacing bulky amino acids with smaller residues such as glycine or alanine to form artificial cavities within the protein environment. Termed cavity mutants, these proteins have the unique ability to bind exogenous ligands either to reconstitute their wild-type activity or to catalyze an unnatural reaction. Initially, this approach focused on the deletion of the proximal ligand and the titration of different exogenous ligands into the proximal cavity in an effort to rescue the catalytic activity of the protein (Figure 22). Pioneered by Barrick for sperm whale myoglobin [202], this method has since been accomplished for CCP [203], heme oxygenase [204], and HRP [205]. For H175G CCP, studies to date have focused on the dynamics of binding unnatural ligands and the resulting effects on catalytic activity. Crystallographic analysis of H175G CCP in the presence of exogenous imidazole shows that the imidazole ligand occupies the same position as the natural histidine, and that there is little deviation in the protein structure [203]. Surprisingly, the imidazole-reconstituted system is devoid of activity despite the binding of the imidazole to the heme in the proximal pocket [203]. An oxo-ferryl species has been generated, although more slowly than for the wild-type [203]. Solid-state deuterium NMR studies investigated whether the unfettering of the proximal ligand from the protein enables it to adopt varied conformations or energetics that alter the pathway or interaction with hydrogen peroxide [206]. No evidence for intermediate ring flipping exchange dynamics or for large angular librations of the ring is observed [206]. Thus, the absence of enzymatic activity is not due to a disordered state for the untethered imidazole.

In an effort to introduce novel substrate oxidation into CCP, the catalytically important Trp191 is replaced with a glycine residue, forming a cavity on the prox-

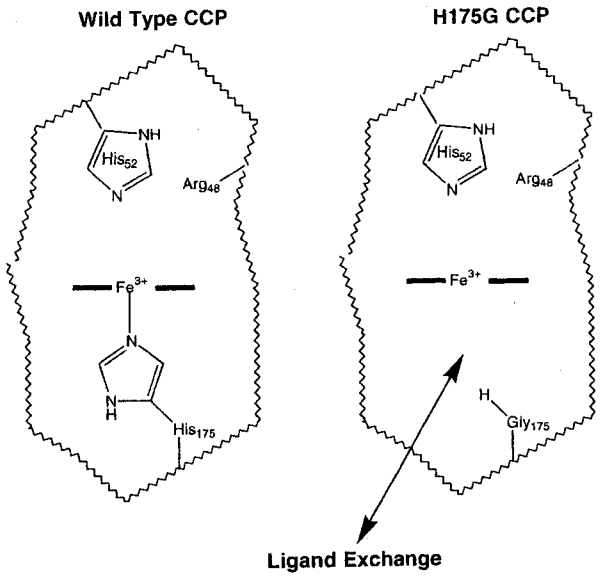

Figure 22. Schematic representation of the active sites of wild-type CCP and the CCP cavity mutant (H175G). Exogenous ligands can be titrated in, or dialyzed out of, the cavity.

imal side of the heme. This buried cavity is able to bind a range of small cationic imidazoles [207], illustrating its ability to stabilize molecules with positive charge. Similar to the imidazoles, 2-aminothiazole (2AT) will also bind within the cavity, as evidenced by calorimetric and crystallographic results [208]. Two separate reactions are observed between 2AT and the oxidized centers of W191G CCP. First, EPR and optical spectra show that 2AT acts as an electron donor to the ferryl center of W191G CCP to reduce it back to the ferric resting state [208]. Second, a less efficient reaction between 2AT and W191G CCP results in the specific covalent modification of Tyr236 [208]. This unexpected result provides the specific assignment of Tyr236 as the site of the alternate radical center when Trp191 is unavailable [208].

Recently, a cavity has been engineered into the distal cavity in an attempt to mimic the oxygenase activity of NOS. Crystallographic and optical studies show that the mutation of Arg48 to an alanine yields a cavity capable of binding N^{ω}-hydroxy-L-arginine (NHA) and *N*-hydroxyguanidine (NHG) [209]. Compound I formation is retained, with as many as three products being observed from the R48A/peroxide-catalyzed oxidation of NHA and NHG [209]. Characterization by mass-spectrometry of the derivatized products of NHA oxidation identified a yellow species as *N*-nitrosoarginine, thus implicating *N*-nitrosoguanidine as the product of NHG oxidation [209]. Therefore, while the hydrogen peroxide-dependent chemistry

catalyzed by R48A CCP has some features in common with that of NOS, namely the ability to oxidize *N*-hydroxyguanidines but not guanidines, the reaction products are clearly distinct from those previously reported for NOS (i.e., cyanamide or N^{δ}-cyanoornithine) [209].

4.5 Conclusions

The relationship between protein structure and function is an area of continuously growing knowledge, as well as problems. The various mechanisms by which oxygenases and peroxidases accomplish their respective reactions are a testament to the reactive versatility of the heme prosthetic group. For P450 enzymes, emerging crystallographic and mechanistic information is moving this field of biochemical research in new and exciting directions. With the growing understanding of how these enzymes interact with their respective substrates, redox partners and—in some cases—the membrane, the rational engineering of P450s may not be far away. Such a stride will enable researchers to tailor this versatile monooxygenase toward specific, biologically active compounds involved in both positive and negative physiological process. In the newer field of NOS research, the recent availability of structural data for two of the three NOS isoforms has helped to create a clearer picture of how this monooxygenase discriminates between active oxygen intermediates in its catalytic mechanism. Presently, mechanistic and mutagenic studies designed to test structure-based proposals are clarifying the role of the heme prosthetic group and the tetrahydrobiopterin in the efficient biosynthesis of nitric oxide. Finally, the recent addition of the crystal structure of HRP to the growing body of structural information on the plant peroxidase superfamily has enabled researchers to compare and contrast the secondary make-up of these versatile oxidases. The roles of many of the catalytic residues conserved across the three classes are now well understood—the result of exhaustive mutagenic and crystallographic studies. The exploitation of CCP as a protein scaffold for the engineering of novel activities and metal binding sites into a peroxidase environment now offers a biological alternative to inorganic model chemistry. The investigation and expansion of this application of rational protein design provides researchers with an opportunity to investigate the structure–function relationships in heme-containing enzymes that differentiate their catalytic activities.

Acknowledgments

We thank Professor Thomas L. Poulos for conveying results from his laboratory prior to publication. Additionally, we thank Drs. Anna-Maria Hays, Mark P. Roach, and Pamela A. Williams for helpful discussions and assistance in the preparation of this review.

Abbreviations

P450	cytochrome P450
P450CAM	camphor-hydroxylating P450 from *Pseudomonas putida*
NADH	nicotinamide adenine dinucleotide
NADPH	nicotinamide adenine dinucleotide phosphate
FAD	flavin adenine dinucleotide
FMN	flavin mononucleotide
P450BM-3	fatty acid-hydroxylating P450 from *Bacillus magaterium*
P450nor	nitric oxide-reducing P450 from *Fusarium oxysporum*
P450TERP	α-terpineol-oxidizing P450 from *Pseudomonas spheroids*
P450eryF	macrolide-hydroxylating P450 from *Saccaropolyspora erythraea*
P4502C5	microsomal P450 from rabbit
EXAFS	extended X-ray absorption fine structure
CCP	cytochrome *c* peroxidase
CPO	chloroperoxidase
•NO	nitric oxide
NOS	nitric oxide synthase
iNOS	inducible NOS
nNOS	neuronal NOS
eNOS	endothelial NOS
Ca^{2+}/CaM	calcium–calmodulin complex
H_4B	tetrahydrobiopterin
H_2B	dihydrobiopterin
L-Arg	L-arginine
NHA	N^{ω}-hydroxy-L-arginine
cGMP	cyclic guaninine monophosphate
H_3B•	one-electron oxidized H_4B
APX	ascorbate peroxidase
LIP	lignin peroxidase
MnP	manganese peroxidase
CIP	peroxidase from *Coprinus cinereus*
PNP	peanut peroxidase
BP 1	barley grain peroxidase
HRP	horseradish peroxidase, isozyme C
BHA	benzhydroxamic acid
FA	C-ferulic acid
CN	cyanide
COX	cytochrome *c* oxidase
2AT	2-aminothiazole
NHG	*N*-hydroxyguanidine

References

1. Durham, B. and Millet, F.S. (1994) in *Encycolpedia of Inorganic Chemistry* (King, R.B.), pp. 1642, Wiley and Sons, Ltd., New York.
2. Walker, F.A. and Simons, U. (1994) in *Encyclopedia of Inorganic Chemistry* (King, R.B.), pp. 1785, Wiley and Sons, Ltd., New York.
3. Dawson, J.H. (1988) *Science 240*, 433–439.
4. Ortiz de Montellano, P.R. (Ed.) (1995) *Cytochrome P450: Structure, Function, and Biochemistry*, 2, Plenum, New York.
5. Dawson, J.H. and Eble, K.S. (1986) in *Advances in Inorganic and Bioinorganic Mechanisms* pp. 1–64, Academic Press, Ltd., London.
6. Sono, M., Roach, M.P., Coulter, E.D. and Dawson, J.H. (1996) *Chem. Rev. 96*, 2841–2887.
7. Antonini, E. and Brunori, M. (1971) *Hemoglobin and Myoglobin in their Reactions with Ligands* (Neuberger, A. and Tatum, E.L.), North-Holland Publishing Co., Amsterdam.
8. Goff, H.M. (1994) in *Encyclopedia of Inorganic Chemistry* (King, R.B.), pp. 1635, Wiley and Sons Ltd., New York.
9. Perutz, M. (1990) in *Mechanisms of Cooperativity and Allosteric Regulation in Proteins* pp. Cambridge University Press, New York.
10. English, A.M. (1994) in *Encyclopedia of Inorganic Chemistry* (King, R.B.), pp. 1682, Wiley and Sons Ltd., New York.
11. Dunford, H.B. (1991) in *Peroxidases in Chemistry and Biology* (Everse, J., Everse, K.E. and Grisham, M.B.), pp. 1, CRC Press, Boca Raton.
12. Marletta, M.A. (1993) *J. Biol. Chem. 268*, 12231–12234.
13. Stuehr, D.J. (1997) *Annu. Rev. Pharmacol. Toxicol. 37*, 339–359.
14. Reynolds, C.H. (1988) *J. Org. Chem. 53*, 6061.
15. Yamamoto, U., Noro, T. and Ohno, K. (1992) *Int. J. Quantum Chem. 42*, 1563.
16. Ghosh, A. (1997) *J. Phys. Chem. B 101*, 3290–3297.
17. Lamoen, D. and Parrinello, M. (1996) *Chem. Phys. Lett. 248*, 309.
18. Matsuzawa, N., Masafumi, A. and Dixon, D. (1995) *J. Phys. Chem. 99*, 7698.
19. Timkovich, R. and Bondoc, L.L. (1990) *Adv. Biophys. Chem. 1*, 203.
20. Mason, H.S., Fawlks, W. and Peterson, J. (1955) *J. Am. Chem. Soc. 77*, 2914.
21. Hayaishi, O., Katagiri, M. and Rothberg, S. (1955) *J. Am. Chem. Soc. 77*, 5450.
22. Hayaishi, O. (1974) in *Molecular Mechanisms of Oxygen Activation* (Hayaishi, O.), pp. 1–28. Academic Press, New York.
23. Garfinkel, D. (1958) *Arch. Biochem. Biophys. 77*, 493.
24. Klingenberg, A. (1958) *Arch. Biochem. Biophys. 75*, 376.
25. Omura, T. and Sato, R. (1964) *J. Biol. Chem. 239*, 2370.
26. Estabrook, R.W., Cooper, D.Y. and Rosenthal, O. (1963) *Biochem. Z. 338*, 741.
27. White, R.E. and Coon, M.J. (1980) *Annu. Rev. Biochem. 49*, 315–356.
28. Gunsalus, I.C., Meeks, J.R., Lipscomb, J.D., Debrunner, P. and Munck, E. (1974) in *Molecular Mechanisms of Oxygen Activation* (Hayaishi, O.), pp. 559–613, Academic Press, New York.
29. Poulos, T.L., Finzel, B.C., Gunsalus, I.C., Wagner, G.C. and Kraut, J. (1985) *J. Biol. Chem. 260*, 16122–16130.
30. Poulos, T.L., Finzel, B.C. and Howard, A.J. (1987) *J. Mol. Biol. 195*, 687–700.
31. Poulos, T.L. (1988) *Pharm. Res. 5*, 67–75.
32. Poulos, T.L. (1995) *Curr. Opin. Struct. Biol. 5*, 767–774.
33. Poulos, T.L., Cupp-Vickery, J.R. and Li, H. (1995) in *Cytochrome P450: Structure, Mechanism, and Biochemistry* (Ortiz de Montellano, P.R.), pp. 125–150, Plenum, New York.
34. Graham, S.E. and Peterson, J.A. (1999) *Arch. Biochem. Biophys. 369*, 24–29.
35. Fulco, A.J. (1991) *Annu. Rev. Pharmacol. Toxicol. 31*, 177–203.
36. Shiro, Y., Fujii, M., Isogai, Y., Adachi, S.-i., Iizuka, T., Obayashi, E., Makino, R., Nakahara, K. and Shoun, H. (1995) *Biochemistry 34*, 9052–9058.
37. Dawson, J.H. and Sono, M. (1987) *Chem. Rev. 87*, 1255–1276.
38. Brewer, C.B. and Peterson, J.A. (1988) *J. Biol. Chem. 263*, 791–798.

39. Pederson, T.C., Austin, R.H. and Gunsalus, I.C. (1977) in *Microsomes and Drug Oxidations* (Ullrich, V., Roots, I., Hildebrandt, A., Estabrook, R.W. and Conney, A.H.), pp. 275–283, Pergamon Press, Oxford, England.
40. Hawkins, B.K. and Dawson, J.H. (1992) *Front. Biotransform. 7*, 216.
41. Porter, T.D. and Coon, M.J. (1991) *J. Biol. Chem. 266*, 13469–13472.
42. Mueller, E.J., Loida, P.J. and Sligar, S.G. (1995) in *Cytochrome P450: Structure, Mechanism and Biochemistry* (Ortiz de Montellano, P.R.), pp. 83–124, Plenum, New York.
43. Loida, P.J. and Sligar, S.G. (1993) *Biochemistry 32*, 11530–11538.
44. Kadkhodayan, S., Coulter, E.D., Maryniak, D.M., Bryson, T.A. and Dawson, J.H. (1995) *J. Biol. Chem. 270*, 28042–28048.
45. Raag, R. and Poulos, T.L. (1992) *Front. Biotransform. 7*, 1–43.
46. Ravichandran, K.G., Boddupalli, S.S., Hasemann, C.A., Peterson, J.A. and Deisenhofer, J. (1993) *Science 261*, 731–736.
47. Hasemann, C.A., Ravichandran, K.G., Peterson, J.A. and Deisenhofer, J. (1994) *J. Mol. Biol. 236*, 1169–1185.
48. Cupp-Vickery, J.R., Li, H. and Poulos, T.L. (1994) *Proteins: Struc. Funct. Genet. 20*, 197–201.
49. Cupp-Vickery, J.R. and Poulos, T.L. (1995) *Nat. Struct. Biol. 2*, 144–153.
50. Park, S.-Y., Shimizu, H., Adachi, S.-I., Nakagawa, A., Tanaka, I., Nakahara, K., Shoun, H., Obayashi, E., Nakamura, H., Iizuka, T. and Shiro, Y. (1997) *Nat. Struct. Biol. 4*, 827–832.
51. Nakahara, K., Shoun, H., Adachi, S., Iizuka, T. and Shiro, Y. (1994) *J. Mol. Biol. 239*, 158–159.
52. Palma, P.N., Moura, I., LeGall, J., Van Beeumen, J., Wampler, J.E. and Moura, J.J.G. (1994) *Biochemistry 33*, 6394–6407.
53. Poulos, T.L., Finzel, B.C. and Howard, A.J. (1986) *Biochemistry 25*, 5314–5322.
54. Poulos, T.L. and Howard, A.J. (1987) *Biochemistry 26*, 8165–8174.
55. Li, H. and Poulos, T.L. (1997) *Nat. Struct. Biol. 4*, 140–146.
56. Raag, R. and Poulos, T.L. (1989) *Biochemistry 28*, 917–922.
57. Raag, R., Martinis, S.A., Sligar, S.G. and Poulos (1991) *Biochemistry 30*, 11420–11429.
58. Vidakovic, M., Sligar, S.G., Li, H. and Poulos, T.L. (1998) *Biochemistry 37*, 9211–9219.
59. Hasemann, C.A., Kurumbail, R.G., Boddupalli, S.S., Peterson, J.A. and Deisenhofer, J. (1995) *Structure 3*, 41–62.
60. Williams, P.A., Cosme, J., Sridhar, V., Johnson, E.F. and McRee, D.E. (2000) *Mol. Cell 5*, 121–131.
61. Schlichting, I., Berendzen, J., Chu, K., Stock, A.M., Maves, S.A., Benson, D.E., Sweet, R.M., Ringe, D., Petsko, G.A. and Sligar, S.G. (2000) *Science 287*, 1615–1622.
62. Dawson, J.H., Kau, L.S., Penner-Hahn, J.E., Sono, M., Eble, K.S., Bruce, G.S., Hager, L.P. and Hodgson, K.O. (1986) *J. Am. Chem. Soc. 108*, 8114–8116.
63. Macdonald, I.D.G., Sligar, S.G., Christian, J.F., Unno, M. and Champion, P.M. (1999) *J. Am. Chem. Soc. 121*, 376–380.
64. Loew, G.H. and Harris, D.L. (2000) *Chem. Rev. 100*, 407–419.
65. Penner-Hahn, J.E., Smith Eble, K., McMurry,T.J., Renner, M., Balch, A.L., Groves, J.T., Dawson, J.H. and Hodgson, K.O. (1986) *J. Am. Chem. Soc. 108*, 7819–7825.
66. Poulos, T.L. (1988) *Adv. Inorg. Biochem 7*, 1–36.
67. Poulos, T.L. and Finzel, B.C. (1984) *Peptide Protein Rev. 4*, 115–171.
68. Sundaramoorthy, M., Choudhury, K., Edwards, S.L. and Poulos, T.L. (1991) *J. Am. Chem. Soc. 113*, 7755–7757.
69. Erman, J.E., Vitello, L.B., Miller, M.A. and Kraut, J. (1992) *J. Am. Chem. Soc. 114*, 6592–6593.
70. Erman, J.E., Vitello, L.B., Miller, M.A., Shaw, A., Brown, K.A. and Kraut, J. (1993) *Biochemistry 32*, 9798–9806.
71. Vitello, L.B., Erman, J.E., Miller, M.A., Mauro, J.M. and Kraut, J. (1992) *Biochemistry 31*, 11524–11535.
72. Dawson, J.H., Holm, R.H., Trudell, J.R., Barth, G., Linder, R.E., Bunnenberg, E., Djerassi, C. and Tang, S.C. (1976) *J. Am. Chem. Soc. 98*, 3707–3708.
73. Sono, M., Andersson, L.A. and Dawson, J.H. (1982) *J. Biol. Chem. 257*, 8308–8320.

74. Sono, M. and Dawson, J.H. (1982) *J. Biol. Chem. 257*, 5496–5502.
75. Liu, H.I., Sono, M., Kadkhodayan, S., Hager, L.P., Hedman, B., Hodgson, K.O. and Dawson, J.H. (1995) *J. Biol. Chem. 270*, 10544–10550.
76. Adachi, S., Nagano, S., Ishimori, K., Watanabe, Y., Morishima, I., Egawa, T., Kitagawa, T. and Makino, R. (1993) *Biochemistry 32*, 241–252.
77. Urano, Y., Higuchi, T., Hirobe, M. and Nagano, T. (1997) *J. Am. Chem. Soc. 119*, 12008–12009.
78. Yi, X., Mroczko, M., Manoj, K.M., Wang, X. and Hager, L.P. (1999) *Proc. Natl. Acad. Sci. USA 96*, 12412–12417.
79. Shimada, H., Kimata, Y., Hirose, T., Kanamori, Y., Toba, Y. and Ishimura, Y. (1995) in *9th International Conference on Cytochrome P450 Biochemistry, Biophysics, and Molecular Biology* eds.), pp. 16, Zurich, Switzerland.
80. Gerber, N.C. and Sligar, S.G. (1994) *J. Biol. Chem. 269*, 4260–4266.
81. Aikens, J. and Sligar, S.G. (1994) *J. Am. Chem. Soc. 116*, 1143–1144.
82. Martinis, S.A., Atkins, W.M., Stayton, P.S. and Sligar, S.G. (1989) *J. Am. Chem. Soc. 111*, 9252–9253.
83. Loida, P.J. and Sligar, S.G. (1993) *Protein Eng. 6*, 207–212.
84. Harris, D.L. and Loew, G.H. (1996) *J. Am. Chem. Soc. 118*, 6377–6387.
85. Imai, M. and Ishimura, Y. (1989) *Proc. Natl. Acad. Sci. USA 86*, 7823.
86. Yeom, H., Sligar, S.G., Li, H. and Poulos, T. (1995) *Biochemistry 34*, 14733–14740.
87. Kimata, Y., Shimada, H., Hirose, T. and Ishimura, Y. (1995) *Biochem. Biophys. Res. Commun. 208*, 96–102.
88. Gerber, N.C. and Sligar, S.G. (1992) *J. Am. Chem. Soc. 114*, 8742–8743.
89. Shimada, H., Makino, R., Unno, M., Horiuchi, T. and Ishimura, Y. (1994) in *Cytochrome P450 8th International Conference* (Lechner, M.C. and Libbey, J., eds.), pp. 299–306, Paris, France.
90. Feldman, P.L., Griffith, O.W. and Stuehr, D.J. (1993) *Chem. Engineer. News December*, 26–38.
91. Marletta, M.A. (1994) *Cell 78*, 927–930.
92. Stuehr, D.J. and Griffith, O.W. (1992) *Adv. Enzymol. Relat. Areas Mol. Biol. 65*, 287–346.
93. Nathan, C. (1992) *FASEB J. 6*, 3051–3064.
94. Masters, B.S.S., McMillan, K., Sheta, E.A., Nishimura, J.S., Roman, L.J. and Martasek, P. (1996) *FASEB J. 10*, 1107.
95. Bredt, D.S. and Snyder, S.H. (1994) *Annu. Rev. Biochem. 63*, 175–195.
96. Bredt, D.S., Hwang, P.M., Glatt, C.E., Lowenstein, C., Reed, R.R. and Snyder, S.H. (1991) *Nature 351*, 714–718.
97. Abusoud, H.M. and Stuehr, D.J. (1993) *Proc. Natl. Acad. Sci. USA 90*, 10769–10772.
98. Siddhanta, U., Presta, A., Fan, B., Wolan, D., Rousseau, D.L. and Stuehr, D.J. (1998) *J. Biol. Chem. 273*, 18950–18958.
99. Ghosh, K. and Stuehr, D.J. (1995) *Biochemistry 34*, 801–807.
100. Crane, B.R., Arvai, A.S., Ghosh, D.K., Wu, C., Getzoff, E.D., Stuehr, D.J. and Tainer. J.A. (1998) *Science 279*, 2121–2126.
101. Fischmann, T.O., Hruza, A., Da Niu, X., Fossetta, J.D., Lunn. C.A., Dolphin, E., Prongay, A.J., Reichert, P., Lundell, D.J., Narula, S.K. and Weber, P.C. (1999) *Nat. Struct. Biol. 6*, 233–242.
102. Raman, C.S., Li, H., Martasek, P., Kral, V., Masters, B.S.S. and Poulos, T.L. (1998) *Cell 95*, 939–950.
103. Narhi, L.O. and Fulco, A.J. (1987) *J. Biol. Chem. 262*, 6683–6690.
104. Rusche, K.M., Spiering, M.M. and Marletta, M.A. (1998) *Biochemistry 37*, 15503–15512.
105. Crane, B.R., Arvai, A.S., Gachhui, R., Wu, C., Ghosh, D.K., Getzoff, E.D., Stuehr, D.J. and Tainer, J.A. (1997) *Science 278*, 425–431.
106. Crane, B.R., Arvai, A.S., Ghosh, S., Getzoff, E.D., Stuehr, D.J. and Tainer, J.A. (2000) *Biochemistry 39*, 4608–4621.
107. Li, H., Raman, C.S., Glaser, C.B., Blasko, E., Young, T.A., Parkinson, J.F., Whitlow, M. and Poulos, T.L. (1999) *J. Biol. Chem. 274*, 21276–21284.
108. Crane, B.R., Rosenfeld, R.J., Arvai, A.S., Ghosh, D.K. Ghosh, A., Tainer, J.A., Stuehr, D.J. and Getzoff, E.D. (1999) *EMBO J. 18*, 6271–6281.

109. Guengerich, F.P. and Macdonald, T.L. (1990) *FASEB J. 4*, 2453–2459.
110. Griffith, O.W. and Stuehr, D.J. (1995) *Annu. Rev. Physiol. 57*, 707–736.
111. Klatt, P., Schmidt, K., Uray, G. and Mayer, B. (1993) *J. Biol. Chem. 268*, 14781–14787.
112. Stuehr, D.J., Kwon, N.S., Nathan, C.F., Griffith, O.W., Feldman, P.L. and Wiseman, J. (1991) *J. Biol. Chem. 266*, 6259–6263.
113. Presta, A., Liu, J., Sessa, W.C. and Stuehr, D.J. (1997) *Nitric Oxide 1*, 74–87.
114. Kwon, N.S., Nathan, C.F., Gilker, C., Griffith, O.W., Matthews, D.E. and Stuehr, D.J. (1990) *J. Biol. Chem. 265*, 13442–13445.
115. Leone, A.M., Palmer, R.M.J., Knowles, R.G., Francis, P.L., Ashton, D.S. and Moncada, S. (1991) *J. Biol. Chem. 266*, 23790–23795.
116. Boggs, S., Huang, L. and Stuehr, D.J. (2000) *Biochemistry 39*, 2332–2339.
117. Hurshman, A.R., Krebs, C., Edmondson, D.E., Huynh, B.H. and Marletta, M.A. (1999) *Biochemistry 38*, 15689–15696.
118. Perry, J. and Marletta, M.A. (1998) *Proc. Natl. Acad. Sci. USA 95*, 1101–1106.
119. Goodwill, K., Sabatier, C., Marks, C., Raag, R., Fitzpatrick, P. and Stevens, R. (1997) *Nat. Struct. Biol. 4*, 578–585.
120. Abu-Soud, H.M., Presta, A., Mayer, B. and Stuehr, D.J. (1997) *Biochemistry 36*, 10811–10816.
121. Clague, M.J., Wishnok, J.S. and Marletta, M.A. (1997) *Biochemistry 36*, 14465–14473.
122. Bec, N., Gorren, A.C.F., Voelker, C., Mayer, B. and Lange, R. (1998) *J. Biol. Chem. 273*, 13502–13508.
123. Ledbetter, A.P., McMillan, K., Roman, L.J., Siler Masters, B.S., Dawson, J.H. and Sono, M. (1999) *Biochemistry 38*, 8014–8021.
124. Presta, A., Siddhanta, U., Wu, C., Sennequier, N., Huang, L., Abu-Soud, H.M., Erzurum, S. and Stuehr, D.J. (1998) *Biochemistry 37*, 298–310.
125. Abu-Soud, H.M., Gachhui, R., Raushel, F. and Stuehr, D.J. (1997) *J. Biol. Chem. 272*, 17349–17353.
126. Welinder, K.G. (1992) *Curr. Opin. Struct. Biol. 2*, 388–393.
127. Smith, A.T. and Veitch, N.C. (1998) *Curr. Opin. Chem. Biol. 2*, 269–278.
128. English, A.M. and Tsaprailis, G. (1995) *Adv. Inorg. Chem. 43*, 79–125.
129. Banci, L. (1997) *J. Biotechnol. 53*, 253–263.
130. Poulos, T.L. (1993) *Curr. Opin. Biotechnol. 4*, 484–489.
131. Poulos, T.L., Freer, S.T., Alden, R.A., Edwards, S.L., Skogland, U., Takio, K., Eriksson, B., Xuong, N.H., Yonetani, T. and Kraut, J. (1980) *J. Biol. Chem. 255*, 575–580.
132. Poulos, T.E. and Kraut, J. (1980) *J. Biol. Chem. 255*, 10322–10330.
133. Edwards, S.L., Poulos, T.L. and Kraut, J. (1984) *J. Biol. Chem. 259*, 12984.
134. Edwards, S.L., Xuong, N.H., Hamlin, R.C. and Kraut, J. (1987) *Biochemistry 26*, 1503–1511.
135. Edwards, S.L. and Poulos, T.L. (1990) *J. Biol. Chem. 265*, 2588–2595.
136. Miller, M.A., Shaw, A. and Kraut, J. (1994) *Nat. Struct. Biol. 1*, 524–531.
137. Pelletier, H. and Kraut, J. (1992) *Science 258*, 1748–1755.
138. Patterson, W.R. and Poulos, T.L. (1994) *J. Biol. Chem. 269*, 17020–17024.
139. Patterson, W.R. and Poulos, T.L. (1995) *Biochemistry 34*, 4331–4341.
140. Mandelman, D., Jamal, J. and Poulos, T.L. (1998) *Biochemistry 37*, 17610–17617.
141. Sundaramoorthy, M., Kishi, K., Gold, M.H. and Poulos, T.L. (1994) *J. Biol. Chem. 269*, 32759–32767.
142. Sundaramoorthy, M., Kishi, K., Gold, M.H. and Poulos, T.L. (1997) *J. Biol. Chem. 272*, 17574–17580.
143. Poulos, T.L., Edwards, S.L., Wariishi, H. and Gold, M.H. (1993) *J. Biol. Chem. 268*, 4429–4440
144. Piontek, K., Glumoff, T. and Winterhalter, K. (1993) *FEBS Lett. 315*, 119–124.
145. Petersen, J.F.W., Kadziola, A. and Larsen, S. (1994) *FEBS Lett. 339*, 291–296.
146. Gajhede, M., Schuller, D.J., Henriksen, A., Smith, A.T. and Poulos, T.L. (1997) *Nat. Struct. Biol. 4*, 1032–1038.
147. Henriksen, A., Schuller, D.J., Meno, K., Welinder, K.G., Smith, A.T. and Gajhede, M. (1998) *Biochemistry 37*, 8054–8060.
148. Henriksen, A., Smith, A.T. and Gajhede, M. (1999) *J. Biol. Chem. 274*, 35005–35011.

149. Schuller, D.J., Ban, N., van Huystee, R.B., McPherson, A. and Poulos, T.L. (1996) *Structure 4(3)*, 311–321.
150. Henriksen, A., Welinder, K.G. and Gajhede, M. (1998) *J. Biol. Chem. 273*, 2241–2248.
151. Ortiz de Montellano, P.R. (1987) *Acc. Chem. Res. 20*, 289–294.
152. Ator, M.A. and Ortiz de Montellano, P.R. (1987) *J. Biol. Chem. 262*, 1542–1551.
153. Ator, M.A., David, S.K. and Ortiz de Montellano, P.R. (1987) *J. Biol. Chem. 262*, 14954–14960.
154. Patterson, W.R., Poulos, T.L. and Goodin, D.B. (1995) *Biochemistry 34*, 4342–4345.
155. Filizola, M. and Loew, G.H. (2000) *J. Am. Chem. Soc. 122*, 18–25.
156. Wirstam, M., Blomberg, M.R.A. and Siegbahn, P.E.M. (1999) *J. Am. Chem. Soc. 121*, 10178–10185.
157. Baek, H.K. and Vanwart, H.E. (1992) *J. Am. Chem. Soc. 114*, 718–725.
158. Sivaraja, M., Goodin, D.B., Smith, M. and Hoffman, B.M. (1989) *Science 245*, 738–740.
159. Scholes, C.P., Liu, Y., Fishel, L.A., Farnum, M.F., Mauro, J.M. and Kraut, J. (1989) *Isr. J. Chem. 29*, 85–92.
160. Miller, M.A., Coletta, M., Mauro, J.M., Putnam, L.D., Farnum, M.F., Kraut, J. and Traylor, T.G. (1990) *Biochemistry 29*, 1777–1791.
161. Newmyer, S.L. and Ortiz de Montellano, P.R. (1995) *J. Biol. Chem. 270*, 19430–19438.
162. Newmyer, S.L. and Demontellano, P.R.O. (1996) *J. Biol. Chem. 271*, 14891–14896.
163. Tanaka, M., Ishimori, K., Mukai, M., Kitagawa, T. and Morishima, I. (1997) *Biochemistry 36*, 9889–9898.
164. Sundaramoorthy, M., Terner, J. and Poulos, T.L. (1995) *Structure 3*, 1367–1377.
165. Sun, W., Kadima, T.A., Pickard, M.A. and Dunford, H.B. (1994) *Biochem. Cell Biol. 72*, 321–331.
166. Nagano, S., Tanaka, M., Ishimori, K., Watanabe, Y. and Morishima, I. (1996) *Biochemistry 35*, 14251–14258.
167. Mukai, M., Nagano, S., Tanaka, M., Ishimori, K., Morishima, I., Ogura, T., Watanabe, Y. and Kitagawa, T. (1997) *J. Am. Chem. Soc. 199*, 1758–1766.
168. Tanaka, M., Nagano, S., Ishimori, K. and Morishima, I. (1997) *Biochemistry 36*, 9791–9798.
169. Smith, A.T., Sanders, S.A., Sampson, C., Bray, R.C., Burke, J.F. and Thorneley, R.N.F. (1993) in *Plant Peroxidases Biochemistry and Physiology, Third International Symposium Proceedings* (Welinder, K.G., Rasmussen, S.K., Penel, C. and Greppin, H.), pp. 159–168, University of Geneva, Geneva.
170. Smulevich, G., Paoli, M., Burke, J.F., Sanders, S.A., Thorneley, R.N. and Smith, A.T. (1994) *Biochemistry 33*, 7398–7407.
171. Rodriguezlopez, J.N., Smith, A.T. and Thorneley, R.N.F. (1996) *J. Biol. Chem. 271*, 4023–4030.
172. Rodriguez-Lopez, J.N., Smith, A.T. and Thorneley, R.N.F. (1996) *J. Inorg Biochem. 1*, 136–142.
173. Vitello, L.B., Erman, J.E., Miller, M.A., Wang, J. and Kraut, J. (1993) *Biochemistry 32*, 9807–9818.
174. Harris, D.L. and Loew, G.H. (1996) *J. Am. Chem. Soc. 118*, 10588–10594.
175. Miller, M.A., Mauro, J.M., Smulevich, G., Coletta, M., Kraut, J. and Traylor, T.G. (1990) *Biochemistry 29*, 9978–9988.
176. Neri, F., Kok, D., Miller, M.A. and Smulevich, G. (1997) *Biochemistry 36*, 8947–8953.
177. Ferrer, J.C., Turano, P., Banci, L., Bertini, I., Morris, I.K., Smith, K.M., Smith, M. and Mauk, A.G. (1994) *Biochemistry 33*, 7819–7829.
178. Sinclair, R., Hallam, S., Chen, M., Chance, B. and Powers, L. (1996) *Biochemistry 35*, 15120–15128.
179. Veitch, N.C., Gao, Y. and Welinder, K.G. (1996) *Biochemistry 35*, 14370–14380.
180. Smulevich, G., Neri, F., Marzocchi, M.P. and Welinder, K.G. (1996) *Biochemistry 35*, 10576–10585.
181. Whitwam, R.E., Koduri, R.S., Natan, M. and Tien, M. (1999) *Biochemistry 38*, 9608–9616.
182. Smulevich, G., Neri, F., Willemsen, O., Choudhury, K., Marzocchi, M.P. and Poulos, T.L. (1995) *Biochemistry 34*, 13485–13490.

183. Choudhury, K., Sundaramoorthy, M., Hickman, A., Yonetani, T., Woehl, E., Dunn, M.F. and Poulos, T.L. (1994) *J. Biol. Chem. 269*, 20239–20249.
184. Nie, G. and Aust, S.D. (1997) *Biochemistry 36*, 5113–5119.
185. Sutherland, G.R., Zapanta, L.S., Tien, M. and Aust, S.D. (1997) *Biochemistry 36*, 3654–3662.
186. Sutherland, G.R.J. and Aust, S.D. (1997) *Biochemistry 36*, 8567–8573.
187. Tanaka, M., Ishimori, K. and Morishima, I. (1998) *Biochemistry 37*, 2629–2638.
188. Pappa, H., Patterson, W.R. and Poulos, T.L. (1996) *J. Inorg. Biochem. 1*, 61–66.
189. Bonagura, C.A., Bhaskar, B., Sundaramoorthy, M. and Poulos, T.L. (1999) *J. Biol. Chem. 274*, 37827–37833.
190. Bonagura, C.A., Sundaramoorthy, M., Bhaskar, B. and Poulos, T.L. (1999) *Biochemistry 38*, 5538–5545.
191. Bonagura, C.A., Sundaramoorthy, M., Pappa, H.S., Patterson, W.R. and Poulos, T.L. (1996) *Biochemistry 35*, 6107–6115.
192. Morimoto, A., Tanaka, M., Takahashi, S., Ishimori, K., Hori, H. and Morishima, I. (1998) *J. Biol. Chem. 273*, 14753–14760.
193. Cheek, J., Mandelman, D., Poulos, T.L. and Dawson, J.H. (1999) *J. Biol. Inorg. Chem. 4*, 64–72.
194. Ortiz de Montellano, P.R., Choe, Y.S., DePillis, G. and Catalano, C.E. (1987) *J. Biol. Chem. 262*, 11641–11646.
195. Savenkova, M.I., Newmyer, S.L. and Ortiz de Montellano, P.R. (1996) *J. Biol. Chem. 271*, 24598–24603.
196. Sigman, J.A., Pond, A.E., Dawson, J.H. and Lu, Y. (1999) *Biochemistry 38*, 11122–11129.
197. Yeung, B.K.S., Wang, X., Sigman, J.A., Petillo, P.A. and Lu, Y. (1997) *Chem. Biol. 4*, 215–221.
198. Wilcox, S.K., Putnam, C.D., Sastry, M., Blankenship, J., Chazin, W.J., McRee, D.E. and Goodin, D.B. (1998) *Biochemistry 37*, 16853–16862.
199. Wang, X. and Lu, Y. (1999) *Biochemistry 38*, 9146–9157.
200. Gengenbach, A., Syn. S., Wang, X. and Lu, Y. (1999) *Biochemistry 38*, 11122–11129.
201. Sigman, J.A., Kwok, B.C., Gengenbach, A. and Lu, Y. (1999) *J. Am. Chem. Soc. 121*, 8949–8950.
202. Barrick, D. (1994) *Biochemistry 33*, 6546–6554.
203. McRee, D.E., Jensen, G.M., Fitzgerald, M.M., Siegel, H.A. and Goodin, D.B. (1994) *Proc. Natl. Acad. Sci. USA 91*, 12847–12851.
204. Wilks, A., Sun, J., Loehr, T.M. and Ortiz de Montellano, P.R. (1995) *J. Am. Chem. Soc. 117*, 2925–2926.
205. Newmyer, S.L., Sun, J., Loehr, T.M. and Ortiz de Montellano, P.R. (1996) *Biochemistry 35*, 12788–12795.
206. Liu, K., Williams, J., Lee, H., Fitzgerald, M.M., Jensen, G.M., Goodin, D.B. and McDermott, A.E. (1998) *J. Am. Chem. Soc. 120*, 10199–10202.
207. Fitzgerald, M.M., Churchill, M.J., McRee, D.E. and Goodin, D.B. (1994) *Biochemistry 33*, 3807–3818.
208. Musah, R.A. and Goodin, D.B. (1997) *Biochemistry 36*, 11665–11674.
209. Hirst, J. and Goodin, D.B. (2000) *J. Biol. Chem. 275*, 8582–8591.
210. Sevrioukova, I.F., Li, H., Zhang, H., Peterson, J.A. and Poulos, T.L. (1999) *Proc. Natl. Acad. Sci. USA 96*, 1863–1868.
211. Gajhede, M., Schuller, D.J., Henriksen, A., Smith, A.T. and Poulos, T.L. (1997) *Nat. Struct. Biol. 4*, 1032–1038.